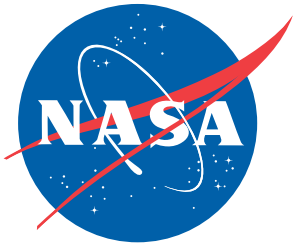
NASA/TM–20210000643



# Experimental and Analytical Characterization of Fluted-Core Sandwich Composite Structures

*Marc R. Schultz*
*Langley Research Center, Hampton, Virginia*

*Leonard Oremont*
*Analytical Mechanics Associates, Inc., Hampton, Virginia*

*Nathaniel W. Gardner*
*Analytical Services & Materials, Inc., Hampton, Virginia*

*J. Carlos Guzman*
*The Boeing Company, Seattle, Washington*

*Douglas McCarville*
*The Boeing Company, Seattle, Washington*

*Mark W. Hilburger*
*Langley Research Center, Hampton, Virginia*

January 2021

# NASA STI Program Report Series

Since its founding, NASA has been dedicated to the advancement of aeronautics and space science. The NASA scientific and technical information (STI) program plays a key part in helping NASA maintain this important role.

The NASA STI program operates under the auspices of the Agency Chief Information Officer. It collects, organizes, provides for archiving, and disseminates NASA's STI. The NASA STI program provides access to the NTRS Registered and its public interface, the NASA Technical Reports Server, thus providing one of the largest collections of aeronautical and space science STI in the world. Results are published in both non-NASA channels and by NASA in the NASA STI Report Series, which includes the following report types:

- TECHNICAL PUBLICATION. Reports of completed research or a major significant phase of research that present the results of NASA Programs and include extensive data or theoretical analysis. Includes compilations of significant scientific and technical data and information deemed to be of continuing reference value. NASA counterpart of peer-reviewed formal professional papers but has less stringent limitations on manuscript length and extent of graphic presentations.

- TECHNICAL MEMORANDUM. Scientific and technical findings that are preliminary or of specialized interest, e.g., quick release reports, working papers, and bibliographies that contain minimal annotation. Does not contain extensive analysis.

- CONTRACTOR REPORT. Scientific and technical findings by NASA-sponsored contractors and grantees.

- CONFERENCE PUBLICATION. Collected papers from scientific and technical conferences, symposia, seminars, or other meetings sponsored or co-sponsored by NASA.

- SPECIAL PUBLICATION. Scientific, technical, or historical information from NASA programs, projects, and missions, often concerned with subjects having substantial public interest.

- TECHNICAL TRANSLATION. English-language translations of foreign scientific and technical material pertinent to NASA's mission.

Specialized services also include organizing and publishing research results, distributing specialized research announcements and feeds, providing information desk and personal search support, and enabling data exchange services.

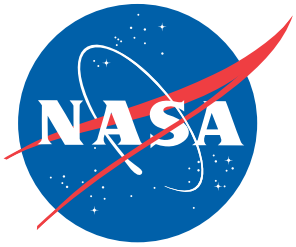
For more information about the NASA STI program, see the following:

- Access the NASA STI program home page at http://www.sti.nasa.gov

- Help desk contact information:

https://www.sti.nasa.gov/sti-contact-form/
and select the "General" help request type.

NASA/TM–20210000643



# Experimental and Analytical Characterization of Fluted-Core Sandwich Composite Structures

*Marc R. Schultz*
*Langley Research Center, Hampton, Virginia*

*Leonard Oremont*
*Analytical Mechanics Associates, Inc., Hampton, Virginia*

*Nathaniel W. Gardner*
*Analytical Services & Materials, Inc., Hampton, Virginia*

*J. Carlos Guzman*
*The Boeing Company, Seattle, Washington*

*Douglas McCarville*
*The Boeing Company, Seattle, Washington*

*Mark W. Hilburger*
*Langley Research Center, Hampton, Virginia*

National Aeronautics and
Space Administration

Langley Research Center
Hampton, Virginia 23681-2199

Januaury 2021

**Acknowledgments**

The work described in this report was conducted as part of the NASA Engineering and Safety Center (NESC) Shell Buckling Knockdown Factor Project, NESC assessment number 07-010-E.

All of the considered test articles were fabricated by The Boeing Company.

The use of trademarks or names of manufacturers in the report is for accurate reporting and does not constitute an official endorsement, either expressed or implied, of such products or manufacturers by the National Aeronautics and Space Administration.

Available from:

NASA STI Program / Mail Stop 148
NASA Langley Research Center
Hampton, VA 23681-2199
Fax: 757-864-6500

## Table of Contents

**1.0 Introduction** ..... **1**

**2.0 Background** ..... **2**

2.1 Fluted-core sandwich composites ..... 2

2.2 Fluted-core sandwich composite analysis approaches ..... 4

**3.0 Experimental Characterization of Fluted-Core Sandwich Composites and Comparison with the Numerical Shell-Noodle Models** ..... **6**

3.1 Coupon Compression Specimens ..... 6

3.2 Transverse-Shear Specimens ..... 15

3.3 Panel Compression Specimens ..... 21

**4.0 Concluding Remarks** ..... **26**

**5.0 References** ..... **26**

## List of Figures

Figure 1. Cross section of a fluted-core composite panel. ..... 3
Figure 2. Solid- and shell-noodle modeling approaches. ..... 5
Figure 3. Coupon compression specimen CP-2A. ..... 7
Figure 4. Load versus strain plots for coupon compression test and analysis. ..... 8
Figure 5. Radial displacement contours of coupon compression specimen CP2-A at the peak failure load (38,597 lb for test and 38,842 lb for analysis). ..... 9
Figure 6. Radial displacement contours of coupon compression specimen CP2-B at the peak failure load (41,948 lb for test and 41,898 lb for analysis). ..... 10
Figure 7. Finite element mesh for coupon compression specimens. ..... 11
Figure 8. Radial displacement traces for coupon compression specimen CP-2A at the peak failure load (38,597 lb for test and 38,842 lb for analysis). ..... 13
Figure 9. Radial displacement traces for coupon compression specimen CP-2B at the peak failure load (41,948 lb for test and 41,898 lb for analysis). ..... 14
Figure 10. Transverse-shear test setup. ..... 16
Figure 11. Transverse-shear FEM. ..... 17
Figure 12. Load versus *y*-direction displacement for the transverse-shear test. ..... 18
Figure 13. Displacement (*x*-direction) contour plots for the transverse-shear test at the peak for a load of 600 lb. ..... 19
Figure 14. Displacement traces for the transverse-shear test. ..... 20
Figure 15. Panel compression test specimen CP-1. ..... 21
Figure 16. Panel compression FEM. ..... 22
Figure 17. Load versus axial displacement for curved-panel compression specimen CP-1. ..... 23
Figure 18. Radial displacement contour plots for the panel compression test at the failure load (117,091 lb for test and 118,938 lb for analysis). ..... 24
Figure 19. Radial displacement traces for the panel compression test at the failure load (117,091 lb for test and 118,938 lb for analysis). ..... 25

## List of Tables

Table 1. Shell-noodle parameters used in FEAs. ..... 12
Table 2. Carbon/epoxy properties used in FEAs. ..... 12

## Nomenclature

| | |
|---|---|
| 3D | Three-dimensional |
| ASTM | American Society for Testing and Materials |
| DIC | Digital image correlation |
| DOF | Degrees of freedom |
| $E_{11}$, $E_{22}$, $E_{33}$ | Laminate Young's Moduli |
| FEA | Finite element analysis |
| FEM | Finite element model |
| $G_{12}$, $G_{13}$, $G_{23}$ | Laminate shear moduli |
| IML | Inner mold line |
| OML | Outer mold line |
| SBKF | Shell Buckling Knockdown Factor |
| TM | Technical Memorandum |
| $\nu_{12}$, $\nu_{13}$, $\nu_{23}$ | Laminate Poisson's Ratios |

Subscripts

| | |
|---|---|
| 1 | Lamina fiber direction |
| 2 | Lamina in-plane transverse direction |
| 3 | Lamina thickness direction |

## Abstract

*As composite materials continue to gain wider acceptance for aerospace primary structures, experimental characterization and analysis methods must evolve, especially if new or underutilized composite structural concepts are to be successfully implemented. One such potentially underutilized concept is the fluted-core sandwich composite, which consists of facesheets separated by angled web members, and has a number of potential advantages over traditional-core (honeycomb, foam, etc.) sandwich composites. However, fluted-core sandwich composites also exhibit behaviors not seen with traditional-core sandwich composites. For example, stable local buckling that can lead to material failure can occur in the facesheets between webs or in the webs themselves. Additionally, in the direction perpendicular to the webs, the effective transverse-shear stiffness is largely determined by the bending stiffnesses of the facesheets and the webs and is generally much lower than in the direction parallel to the webs. These local buckling and transverse-shear behaviors can have a large influence on material failure and global buckling, respectively. Thus, it is important to accurately characterize and model these behaviors. In this report, a series of experiments designed to elicit some of these fluted-core sandwich composite structural responses is discussed and the results are compared with results from a previously developed finite element analysis approach; qualitative and quantitative agreement between the experiment and analysis is shown.*


## 1.0 Introduction

Originally, most launch vehicle primary structures were fabricated of metallic materials. More recently, composite materials have gained and continue to gain wider acceptance for such primary structures. For example, the in-service Delta II, Delta IV, Atlas V, Antares, Ariane 5, Ariane 6, and Vega launch vehicles all utilize composite structures, as will the Vulcan family of launch vehicles.[1,2,3] However, a number of additional design and analysis challenges are encountered when designing with composites—one needs to consider ply angles, more complicated failure modes, and increased potential for difficult-to-detect damage or flaws. As evidenced by the successful use of composites in a growing number of launch vehicle applications, methods have been developed to address these design and analysis challenges for certain composite constructions. However, new or underutilized composite constructions can require the development of additional characterization (design, analysis, and test) methods. The results of structural experimental testing are compared with predictions from a previously developed finite element analysis method for one such construction, the fluted-core sandwich composite, are discussed herein.

Background is given in Section 2.0 of this Technical Memorandum (TM)—a history and description of fluted-core sandwich composites and similar constructions is given in Section 2.1, and a description of analysis methods is given in Section 2.2. In Section 3.0 of this TM, the considered experimental tests are described, and results are compared with finite element predictions. Coupon compression tests are discussed in Section 3.1, a novel transverse-shear test is discussed in Section 3.2, and a larger panel compression test is discussed in Section 3.3. In the

discussion of these tests and test-analysis correlation, the primary focus is on the stiffness-related responses rather than on failure. Concluding remarks are given in Section 4.0.

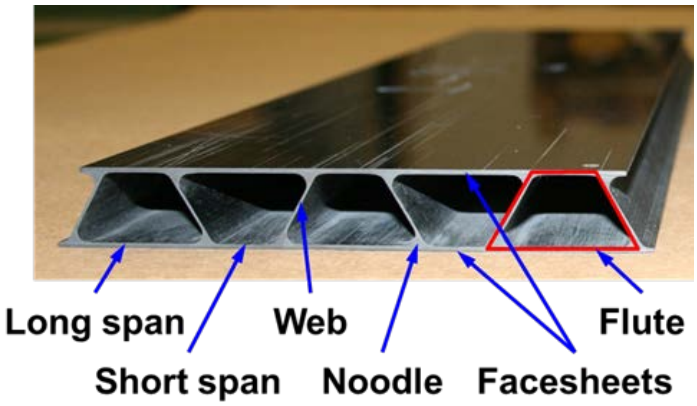
# 2.0 Background

## 2.1 Fluted-core sandwich composites

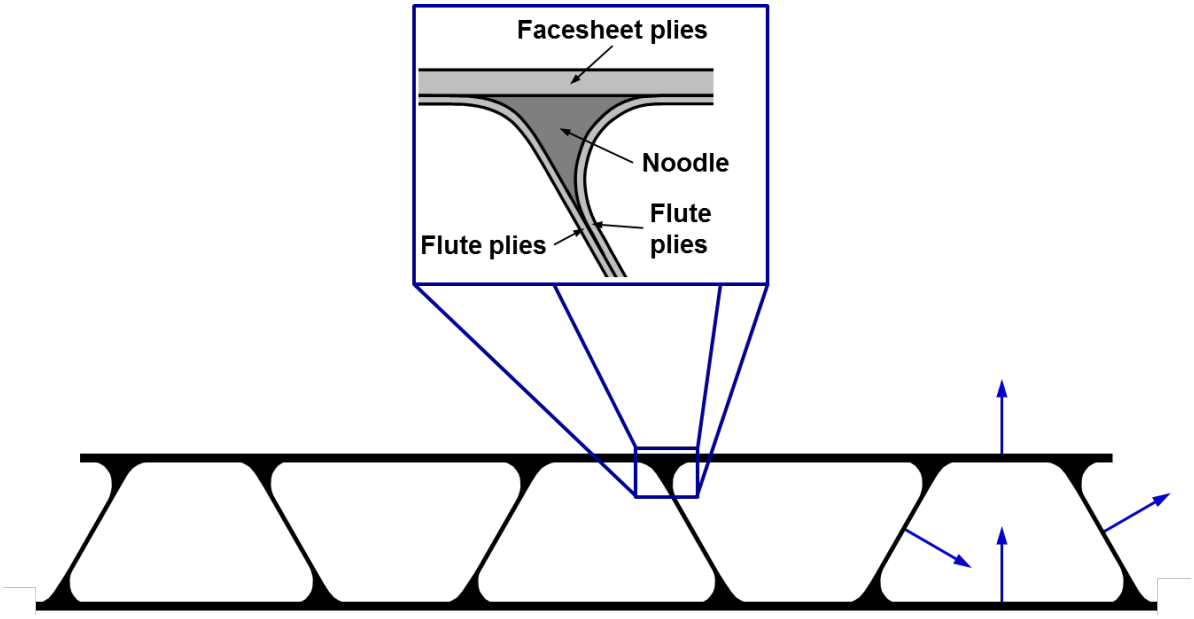
Sandwich structures, which consist of high-strength and high-stiffness facesheets separated by a lightweight core, often trade very well for stability-critical shell structures such as launch vehicle intertanks, interstages, skirts, and shrouds. However, there are some manufacturing and in-service drawbacks to traditional foam- or honeycomb-core sandwich composite structures that may be alleviated by using less common sandwich composite constructions such as the fluted-core sandwich composite concept.[4] The fluted-core sandwich composites (Figure 1) discussed herein are similar to traditional sandwich composites in that they consist of facesheets separated by a lightweight core, but the lightweight core consists of composite web members and unidirectional radius fillers, or noodles, where the webs meet the facesheets.

Fluted-core, corrugated-core, and similar sandwich structures (collectively called structured-core) have been considered for use in aerospace applications for many years. For example, as early as the 1940s, metallic corrugated-core was used on commercial aircraft[5] and later considered for space applications.[6] In order to facilitate structured-core designs, expressions for the elastic constants were derived and experimentally validated.[7,8,9,10] During this work, it was recognized that local plate-buckling-type instabilities in the webs and in the faces between the webs could occur under certain loading conditions.[9,11] Further investigations on similar metallic cellular-core sandwich shells have continued since these early studies [e.g., refs. 12–17].

As composites became more viable for structural applications, fluted-core and other structured-core sandwich composites have been explored. For example, Jegley studied the structural efficiency of fluted-core sandwich composite panels by developing optimized designs for compression-loaded panels.[18] Collier formulated expressions for the stiffnesses of structured-core composite panels and used these to represent the panels as equivalent anisotropic finite element plates.[19,20] Composite structured-core structures were considered by a number of investigators for integrated space-vehicle thermal protection systems,[21,22,23] and for purgeable cryogenic tank structure.[24] Recently, Boorle and Mallick explored the influences of geometric parameters and laminate stacking sequence on the equivalent plate properties of fluted-core-type sandwich composite plates.[25,26] In 2015, Dayyani, et al. provided a fairly extensive review of composite structured-core sandwich shells with application to morphing structures.[27] Others, such as Zangani, et al., Bednarcyck, et al., and Tumino, et al., have investigated foam-filled structured-core composite sandwich panels.[28,29,30]




a) Fluted-core cross section.




b) Sketch detailing noodle region and the shell normals.

Figure 1. Cross section of a fluted-core composite panel.

Though composite fluted-core and structured-cores have been studied for many years, recent manufacturing improvements have made their implementation more practical. Studies have indicated that fluted-core has several manufacturing and in-service benefits over traditional honeycomb core for sandwich composites.[4] Recently, a fluted-core sandwich design was used in the construction of a 5.5-m-diameter composite cryotank built by The Boeing Company and tested by NASA.[31-34] Additionally, the Boeing Company produced and provided to NASA a 4-m-diameter fluted-core barrel designed as a shell-buckling test article for the NASA Shell Buckling Knockdown Factor (SBKF) project.[35] It was in the process of designing, analyzing, and testing related to this 4-m test article that the observations and testing that are discussed in this report were made.

The fluted-core sandwich concept has perceived advantages and is being used in developmental launch vehicle structures, so an improved understanding of the structural response of fluted-core sandwich composites is needed before they can gain widespread application. For example, when loaded in compression, and as was observed in metallic structured-core sandwich structures,

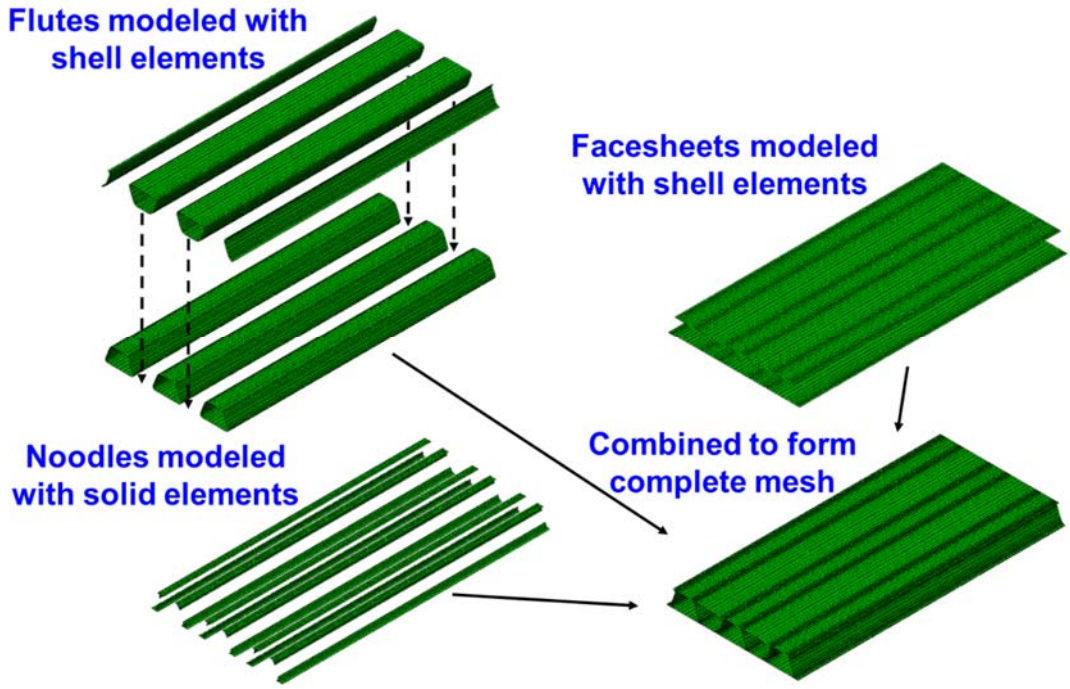
fluted-core sandwich composite panels can locally buckle in the facesheet spans between noodles or in the webs before material failure occurs,[4] and the predicted load for this local buckling is highly dependent on how the noodle at the intersection of the webs and faces is modeled. The transverse-shear stiffness of fluted-core sandwich composites is typically quite stiff in the direction of the flutes; however, the effective transverse-shear stiffness is fairly low in the direction perpendicular to the flutes—what would be the circumferential direction in a cylindrical shell. Additionally, it has long been known that the transverse-shear stiffness can be important in determining the global buckling behavior of sandwich cylinders (see, for example, ref. 36). Because the effective circumferential transverse-shear stiffness is largely influenced by bending of the facesheets and the webs, and the rigidity of the connection between the facesheets and the webs, the method of modeling the noodle is also important when trying to predict circumferential transverse-shear stiffness and global buckling behavior of fluted-core sandwich cylinders. Preliminary results indicate that properly accounting for transverse-shear compliance may reduce predicted global cylinder bifurcation-buckling loads by 30% or more when compared to a model with infinite transverse-shear stiffness.[37]

## 2.2 Fluted-core sandwich composite analysis approaches

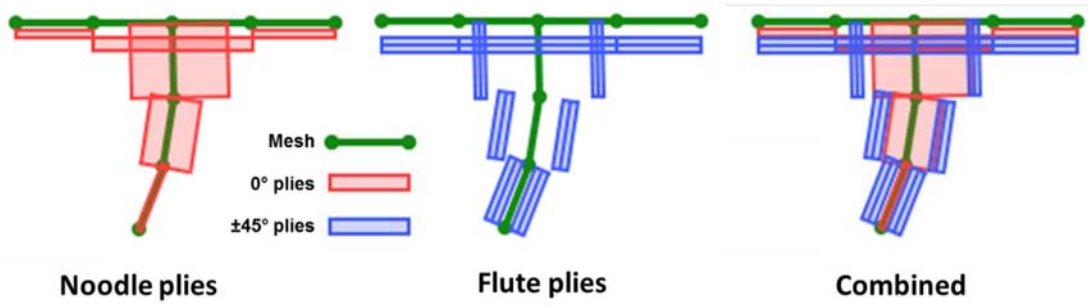
It might be tempting to either ignore the noodles or use beam elements to model the noodles because of the relatively small cross-sectional area of the noodles with respect to the remainder of the test article. The noodle generally cannot be ignored because the unidirectional material can provide a significant portion of the stiffness in the direction of the fluted core. Additionally, the noodle dimensions, though small, are not negligible when compared to the flute dimensions, and if the noodle is modeled as a beam, the unsupported facesheet dimension between noodles will be too long and the stiffness of the web-to-face connection will be underpredicted. Thus, a beam-noodle approach will lead to underpredicted local buckling loads due to the underpredicted effective transverse-shear stiffness. If a more accurate assessment of performance is desired, the noodle needs to be accurately represented. One approach, that has been shown to provide excellent correlation with experimental data, is to represent the faces and webs with shell elements and the noodle with three-dimensional (3D) solid elements (ref. 4 and Figure 2a). This approach, however, is very computationally intensive and not practical for large or complicated structures. Therefore, a more computationally efficient approach that models the faces, webs, and noodles all with shell elements has been developed and shown to agree well with the solid-noodle approach.[38,39] In this report, the results of the more efficient *shell-noodle* modeling approach of ref. 39 will be compared with experimental results for several specimen configurations.

In the shell-noodle modeling approach, the entire noodle region (noodle and flute plies) is modeled using shell elements. As shown in Figure 2b, the cross section of the noodle region is collapsed to the shape of a “T” made of seven mesh segments in cross section where the leg of the “T” essentially bisects the original (curved) triangular shape of the noodle and the top of the “T” is coincident with the facesheet shell elements. In each of the seven mesh segments, coincident shell elements separately representing the noodle and flute plies are meshed on the same nodes. Each of these shell elements is defined with a thickness and an offset so there are a total of 14 geometric parameters to be determined in the noodle region. Because the 45° plies in the noodle overlap in this shell-noodle approach and are therefore over represented, the thickness of the 45° plies in the web element closest to the facesheets was added as a fifteenth parameter with the expectation that this thickness would be reduced to an almost negligible value. Finally, the offsets of the 45° plies were added as additional parameters. Therefore, a total of 22 parameters were considered to define

the shell-noodle model. This shell-noodle representation is clearly a simplification of the physical noodle-region geometry, but it can be imagined that the proper selection of these geometric parameters will produce predicted structural responses similar to those obtained with the solid-noodle model. This concept is then used in the shell-noodle modeling approach—specifically, the geometric parameters in the shell-noodle model are varied in a heuristic way until certain predicted structural responses match, within chosen tolerances, those of the solid-noodle approach as described in ref. 39. Once these structural responses match, the shell-noodle model is considered "mechanically equivalent" to the solid-noodle model. The assumption is then that the shell properties thus determined can be used to model a much larger, complex structure made with the same noodle, flute and facesheet geometries, and materials.




a) Solid-noodle modeling approach.




b) Shell-noodle modeling approach.

Figure 2. Solid- and shell-noodle modeling approaches.

# 3.0 Experimental Characterization of Fluted-Core Sandwich Composites and Comparison with the Numerical Shell-Noodle Models

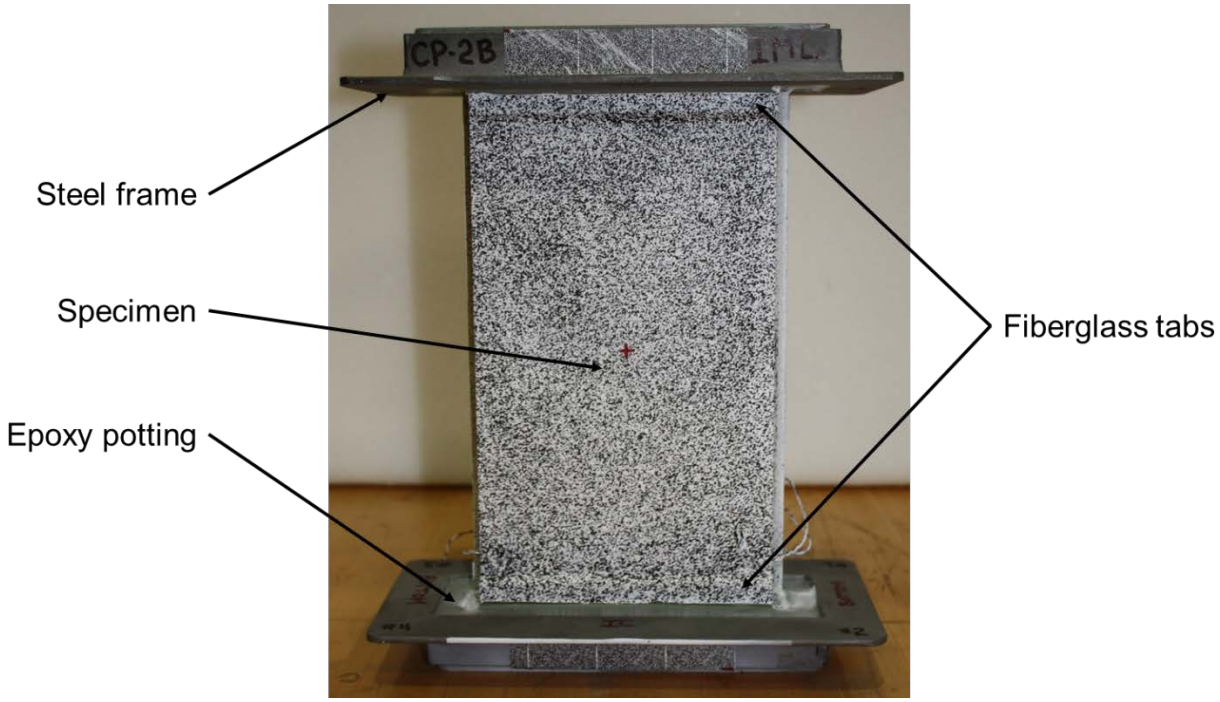
Three specimen types, which were designed to interrogate different fluted-core sandwich composite structural responses, were tested. These specimen types were

- Coupon compression specimens to determine the material stiffness and examine the axial compression and local buckling responses
- Shear specimen to examine the effective transverse-shear behavior
- Curved-panel compression specimen to examine the global bending response

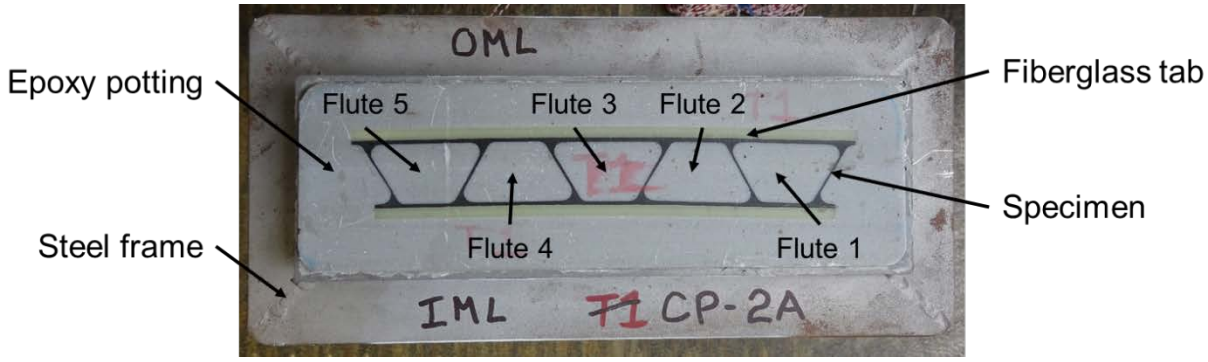
It should be noted that the test and analysis efforts described in this and in previous papers by the authors[4,38,40] were part of a development effort for fluted-core sandwich composite structures; and specimens were fabricated using available, but not necessarily the same, material. All specimens considered herein were manufactured by the Boeing Company as part of a single 4-m-diameter quarter-cylinder panel with the flute cells aligned with the axial direction. The quarter-cylinder panel was manufactured from 350°F-cure toughened carbon-epoxy prepreg by placing a prepreg facesheet on a curved female mandrel, wrapping prepreg around trapezoidal flute mandrels and arranging those mandrels with pultruded uncured noodles over the prepreg facesheet, and then applying the second facesheet. This entire assembly was then autoclave co-cured and the flute mandrels were removed after cure. With the exception of the global cylindrical curvature of the current test articles, the cross-section was essentially the same as the subscale cross section from Refs. 4, 38, and 40. That is, the test articles were 0.74 in. thick and the trapezoidal mandrel radii for the noodles were 0.1 in. The total web layup was $[+45/-45/+45/-45]_T$ and the total facesheet layup (including the plies originally wrapped around the mandrels) was $[+45/-45/0/90]_S$. (Note: The coordinate systems for describing the layouts use 0° as the long longitudinal test-article direction, 90° in plane and perpendicular to the 0° direction, and normals as shown by the arrows in Figure 1b.) It should also be noted that during fabrication, the noodles were oversized by 18% to help ensure that there were no voids or resin-rich regions associated with the noodle region.

## 3.1 Coupon Compression Specimens

The compression performance parallel to the flutes is perhaps the most important structural performance metric because the fluted-core sandwich composite construction is being considered for cylindrical structures loaded primarily in axial compression. In order to characterize the local compression response, 11.0-in.-long coupon compression specimens (Figure 3) with five flutes were fabricated and tested. On each end, 1.5-in.-long fiberglass tabs were bonded on the exterior surfaces and 1.0 in. at each end was potted in an epoxy grout as shown. These compression specimens were designed such that they would not exhibit global panel-type buckling under axial compression loading. In Reference 4, it was shown that as similar specimens were loaded, they locally buckled in the facesheet wide spans and in the webs. Because these buckles locally increased the compression strain, failure consistently occurred through the peaks of the buckling half waves. Therefore, it is important to consider such buckling if one wants to accurately predict material failure.




a) IML side view.




b) Top cross-sectional view.

Figure 3. Coupon compression specimen CP-2A.

Two coupon compression specimens were tested as part of the current effort. These test articles were designated CP2-A and CP2-B and were cut from a larger previously tested panel similar to the curved-panel compression specimen discussed in Section 3.3. Axial strain gages were applied to both the outer mold line (OML) and inner mold line (IML) 1.0 in. above the bottom fiberglass tabs centered in flutes 1 and 5 (Figure 3b), and a black-and-white speckle pattern was painted on the specimen for full-field displacement measurements using three-dimensional digital image correlation (DIC) techniques.[41]

The global stiffness responses of the two coupon compression specimens can be examined by plotting the compressive load versus the average strain from the four axial strain gages (Figure 4). In this figure, the red curve represents specimen CP2-A and the blue curve represents CP2-B. As indicated by the termination of these curves, specimen CP2-A failed at a load of 38,597 lb and specimen CP2-B failed at a load of 41,948 lb (9% higher). Despite this difference in failure load, the prefailure load-versus-strain responses of the two specimens were nearly identical. These

responses were initially linear, but showed increasing nonlinearity at loads over 35,000 lb. This nonlinearity is shown in Figure 4 as an apparent stiffening, but is really an indication of local buckling in the wide spans of flute faces. The local buckling can be seen at its most fully developed stage by looking at the radial displacement contours at the peak failure load (Figure 5 for CP2-A and Figure 6 for CP2-B). In these figures, it is shown that local buckling developed in each of the wide spans (flutes 1, 3, and 5 on the OML and flutes 2 and 4 on the IML) at the ends of the specimen. In each case, these buckles initiated with an inward dimple moving toward the midsurface in the specimen just past the tabs. As the load increased, additional buckles developed along the length of the flute wide spans.

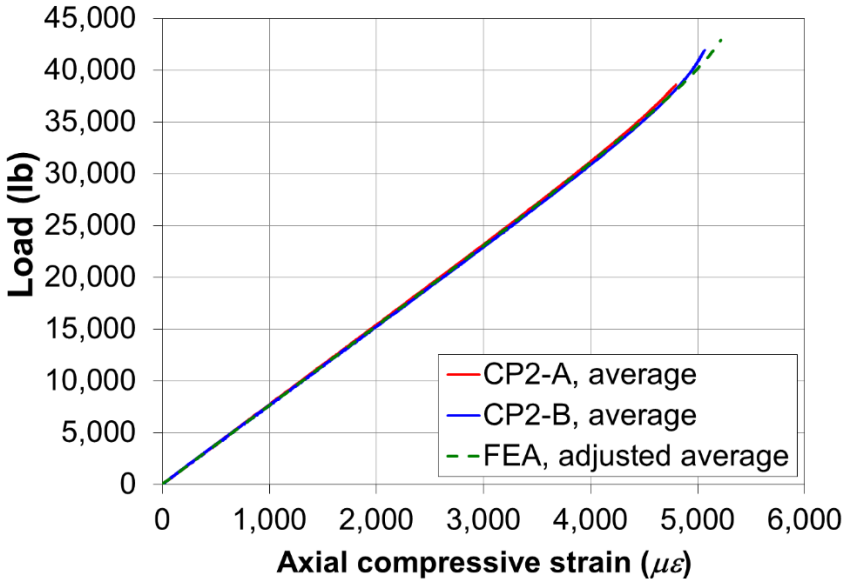
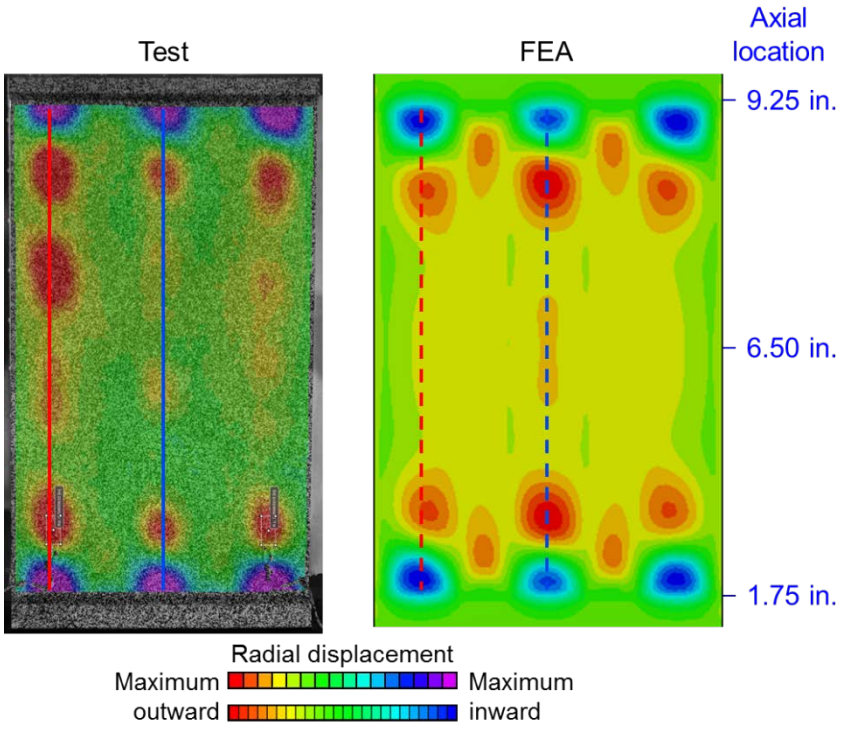
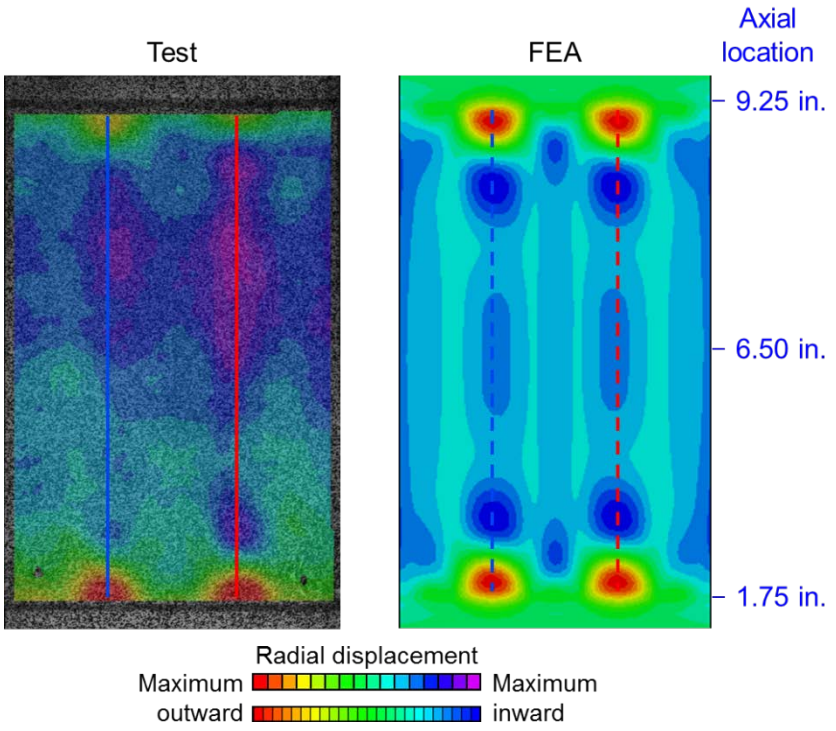



Figure 4. Load versus strain plots for coupon compression test and analysis.

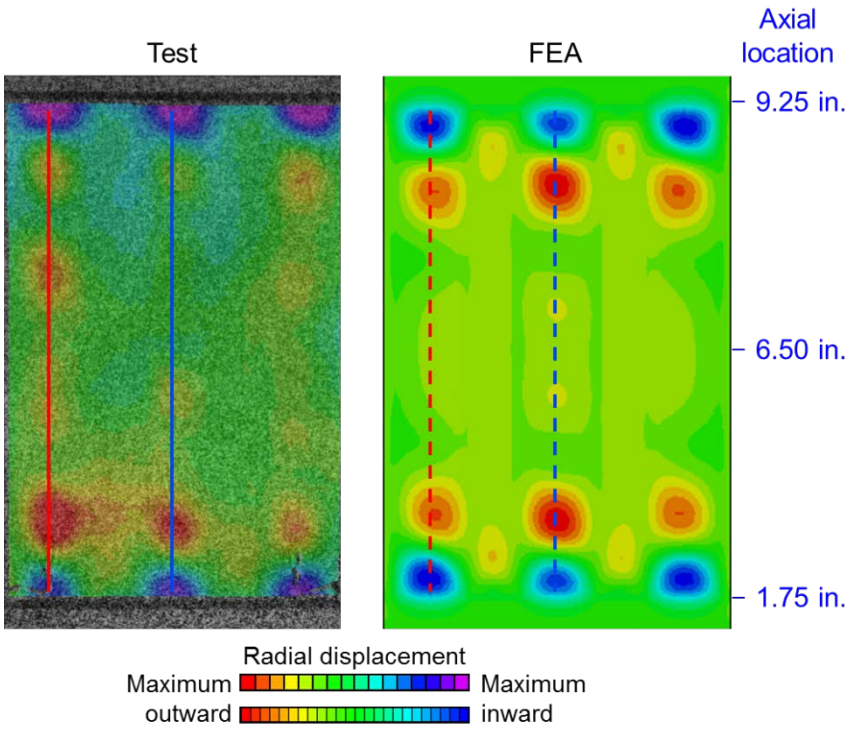



a) OML.

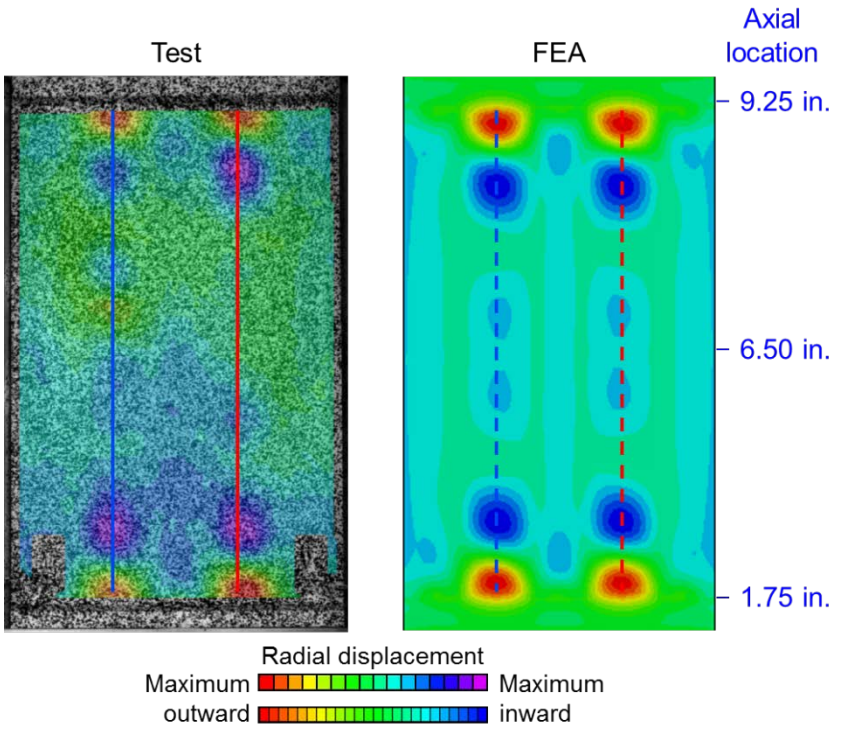



b) IML.

Figure 5. Radial displacement contours of coupon compression specimen CP2-A at the peak failure load (38,597 lb for test and 38,842 lb for analysis).




a) OML.




b) IML.

Figure 6. Radial displacement contours of coupon compression specimen CP2-B at the peak failure load (41,948 lb for test and 41,898 lb for analysis).

The finite element model (FEM) created to analyze the compression response of these coupon specimens is shown in Figure 7, had 38,720 elements, 15,488 nodes, and 92,928 degrees of freedom (DOF). This model and the other models discussed in this document were created with the finite element pre- and post-processing software Patran®[42] and analyzed with the general-purpose finite element software Abaqus.[43] As discussed in ref. 39, the shell-noodle coupon compression model was developed and tuned by comparing the structural responses with a more computationally intensive 3D solid model of the noodle, herein termed the solid-noodle model. With both the solid- and shell-noodle models, the noodle fiber-direction stiffness was increased by 18% to account for the extra material placed in that region during fabrication. The shell-noodle parameters developed in ref. 39 are given in Table 1.

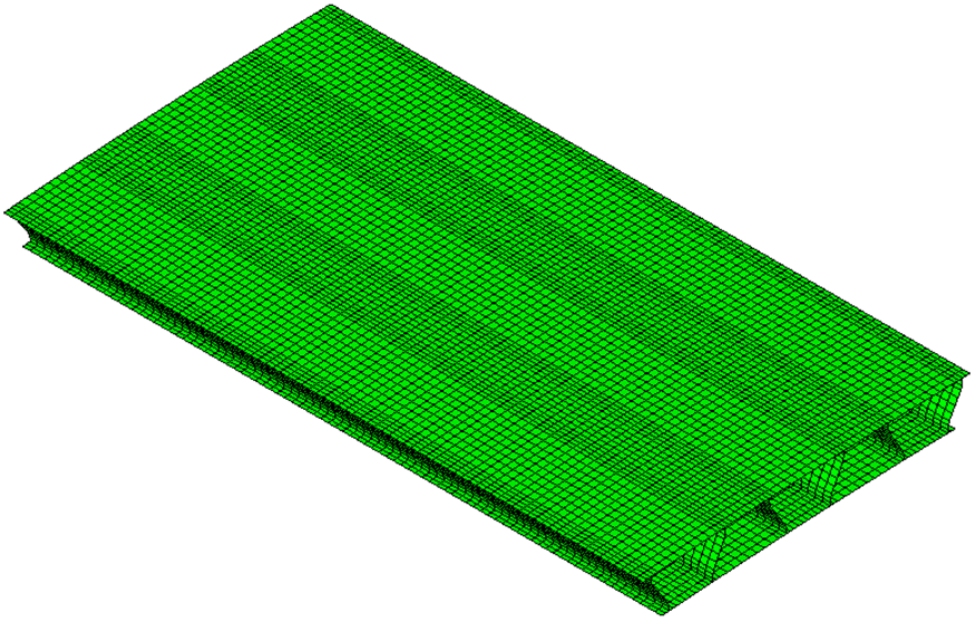


Figure 7. Finite element mesh for coupon compression specimens.

Because of the developmental aspect of this effort, material properties for the material were not well known so material properties for another well-known intermediate modulus carbon-epoxy system were used in initial analyses (Table 2). The fiberglass tabs were assumed to be isotropic with a Young's Modulus of $2.7 \times 10^6$ psi and Poisson's Ratio of 0.3. When compared with the experimental stiffness data shown in Figure 4, the finite element analysis (FEA) predicted response was too soft. Therefore, all terms of the carbon-epoxy stiffnesses used in the analysis were increased by 4% to match the linear portion of the experimental data, and these stiffnesses were used to generate the analysis results discussed in this report. The load versus average strain curve for the FEA with the adjusted material properties is shown in Figure 4. (Throughout this report, the test results are given by solid lines and the FEA results are given by dashed lines.) As with the test data, the FEA response shows nonlinearity increasing after 35,000 lb, but more nonlinearity was seen during the tests. As mentioned earlier, this nonlinearity is due to local buckling under the strain gages. The FEA did not consider material failure, but the radial displacement contour plots for the FEA at loads similar to the test articles are shown in Figure 5 and Figure 6. The FEA was able to qualitatively capture the displacement response of the test articles in that local buckling was represented with inward dimples near the tabs in each of the long spans and that the local buckling became more pronounced along the length of the long spans as the load was increased.

This increase in the local buckling can be seen by observing that the pattern is more developed in the higher-loaded Figure 6 sample CP2-B than it is in the Figure 5 sample CP2-A. Though not shown, these local buckling patterns are predicted to be fully developed with essentially equal-amplitude buckles distributed evenly along each flute long span by a load of 48,000 lb. To quantitatively compare the FEA results with the tests, radial displacement traces are plotted in Figure 8 and Figure 9 for DIC data extracted from the specimen faces at the locations indicated by the vertical lines in Figure 5 and Figure 6, that is, for data extracted along the center of flutes 1 and 3 on the OML and along flutes 2 and 4 on the IML. (It should be noted that both the OML and IML test data in Figure 8 were shifted 0.009 in. in the radial outward direction in an attempt to remove rigid body motion in the test that could not have been anticipated in the FEA.) It is generally observed that the magnitude of the radial deformations and local buckling response of midsection were predicted well with the FEA, but the total amplitude was underpredicted. In particular, the radial deformation magnitudes near the tabs were significantly underpredicted, particularly on the OML side. This general underprediction may indicate that the method of modeling the tab was too stiff. A too-stiff tab could also account for the local buckling in the predictions seeming to develop at higher loads than was seen in test. Despite the differences, the radial displacement traces indicate that with increasing load a total of nine half waves were developing in each of the flute long spans for both test and FEA.

Table 1. Shell-noodle parameters used in FEAs.

| | **Segment** | | | | | | |
|---|---|---|---|---|---|---|---|
| **Property** | **F1** | **F2** | **F3** | **F4** | **W1** | **W2** | **W3** |
| Noodle ply thickness (in.) | 0.00601 | 0.01226 | 0.01226 | 0.00601 | 0.07500 | 0.04700 | 0.00200 |
| Noodle shell fractional offset | 0.9900 | 1.2500 | 1.2500 | 0.9000 | 0.0600 | 0.0268 | 0.3000 |
| Flute ply thickness (in.) | 0.00560 | 0.00560 | 0.00560 | 0.00560 | 0.00450 | 0.00560 | 0.00560 |
| Flute shell fractional offset | 2.4000 | 2.3380 | 2.3380 | 2.4000 | 6.0000 | 3.5000 | 0.6580 |

Segment locations:

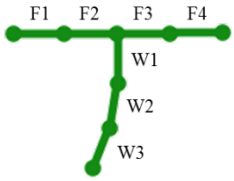
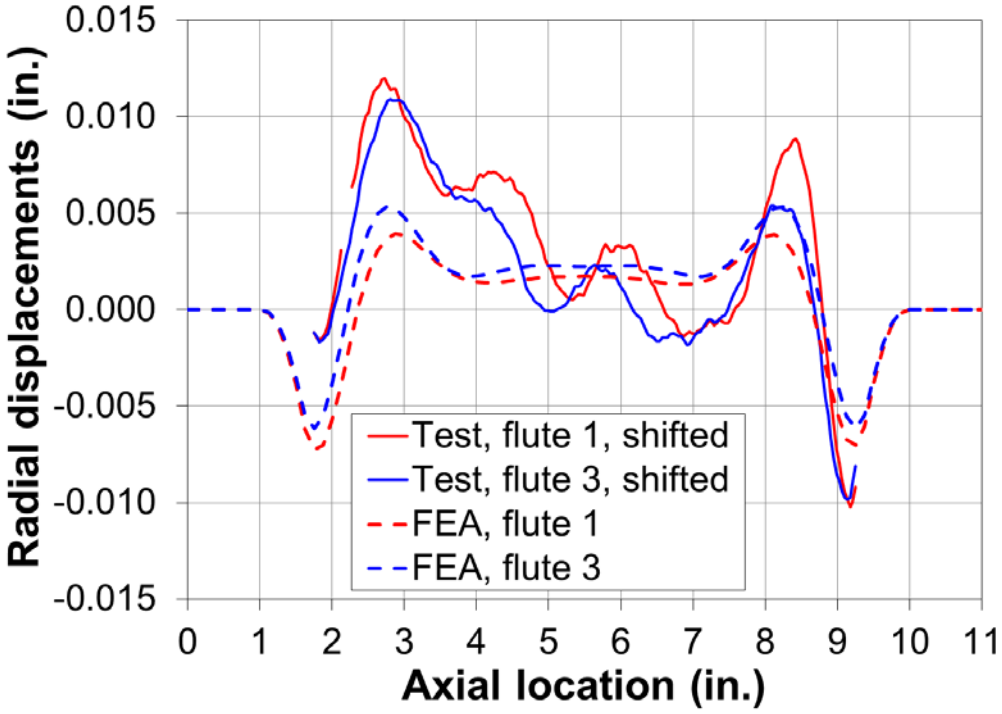
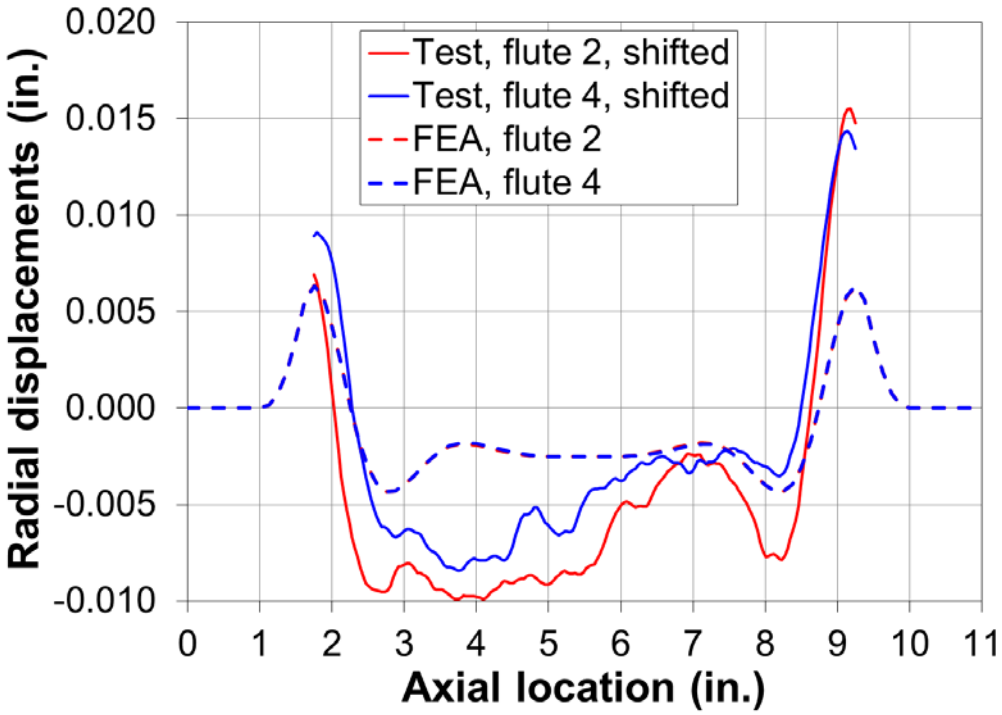



Table 2. Carbon/epoxy properties used in FEAs.

| **Property** | **Baseline Tape** | **Updated Tape** | **Baseline Pultruded** | **Updated Pultruded** |
|---|---|---|---|---|
| $E_{11}$ (compression) | 2.12E+7 psi | 2.2048E+7 psi | 2.12E+7 psi | 2.6017E+7 psi |
| $E_{22}$ (compression) | 1.82E+6 psi | 1.8928E+6 psi | 1.82E+6 psi | 1.8928E+6 psi |
| $E_{33}$ (compression) | 1.35E+6 psi | 1.4040E+6 psi | 1.82E+6 psi | 1.8928E+6 psi |
| $E_{11}$ (tension) | 2.35E+7 psi | 2.4440E+7 psi | | |
| $E_{22}$ (tension) | 1.67E+6 psi | 1.7368E+6 psi | | |
| $E_{33}$ (tension) | 1.35E+6 psi | 1.4040E+6 psi | | |
| $\nu_{12}$ | 0.311 | 0.311 | 0.311 | 0.311 |
| $\nu_{13}$ | 0.311 | 0.311 | 0.311 | 0.311 |
| $\nu_{23}$ | 0.500 | 0.500 | 0.500 | 0.311 |
| $G_{12}$ | 7.30E+5 psi | 7.5920E+5 psi | 7.30E+5 psi | 7.5920E+5 psi |
| $G_{13}$ | 6.40E+5 psi | 6.6560E+5 psi | 6.40E+5 psi | 6.6560E +5 psi |
| $G_{23}$ | 3.30E+5 psi | 3.4320E+5 psi | 6.40E+5 psi | 6.6560E +5 psi |

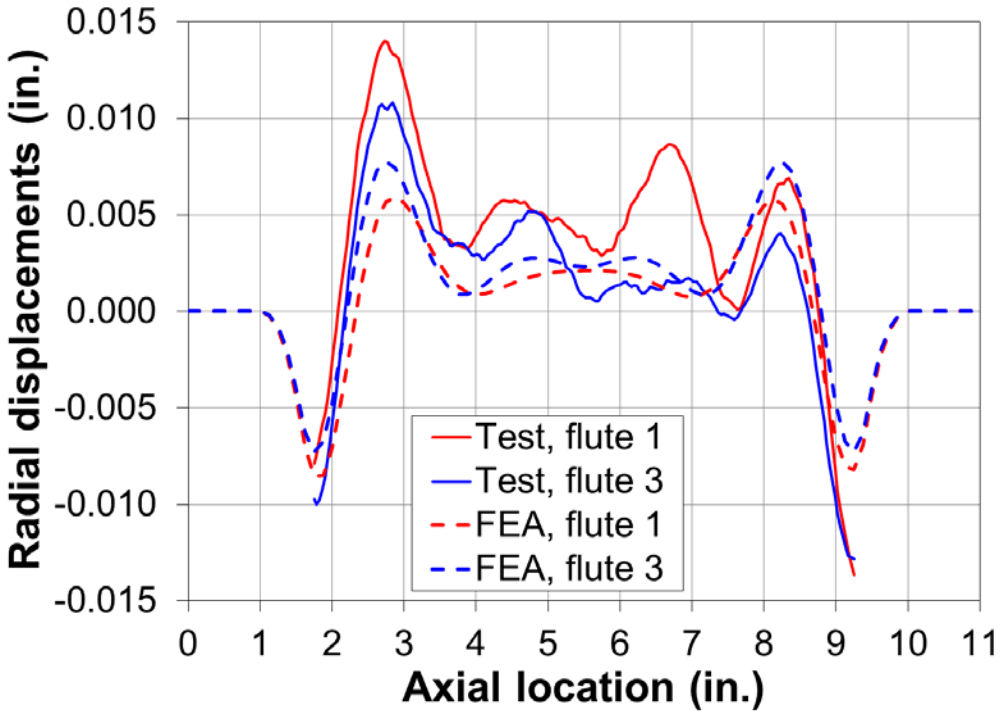



a) OML.

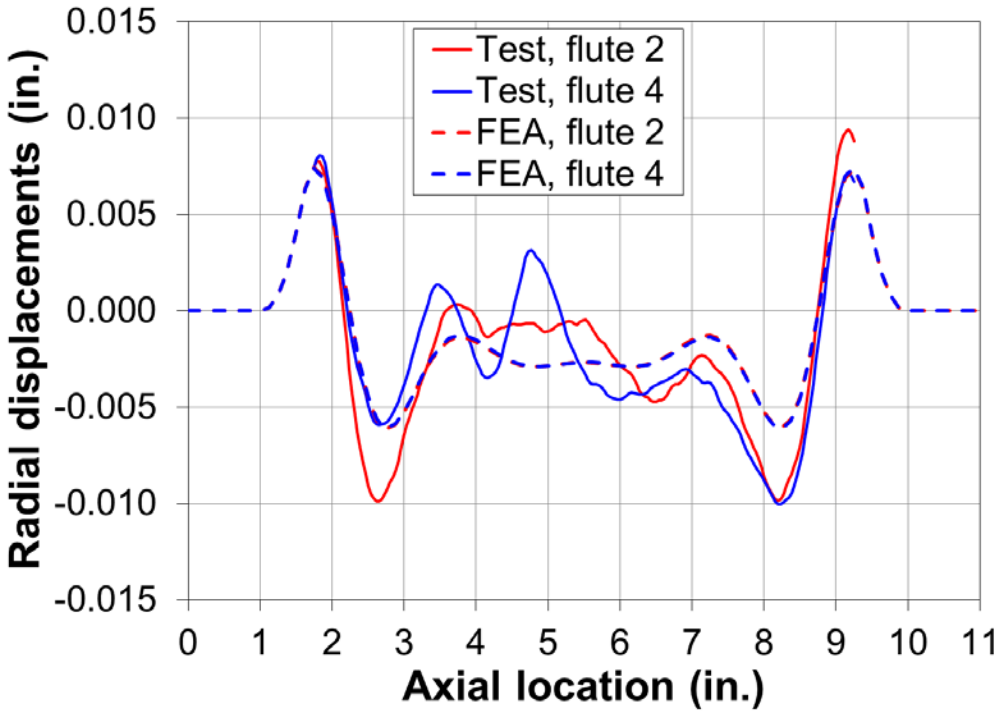



b) IML. (Note that the FEA flute 2 and flute 4 results are nearly coincident.)

Figure 8. Radial displacement traces for coupon compression specimen CP-2A at the peak failure load (38,597 lb for test and 38,842 lb for analysis).




a) OML.




b) IML. (Note that the FEA flute 2 and flute 4 results are nearly coincident.)

Figure 9. Radial displacement traces for coupon compression specimen CP-2B at the peak failure load (41,948 lb for test and 41,898 lb for analysis).

### 3.2 Transverse-Shear Specimens

As discussed in Section 1.0, the effective transverse-shear stiffness of a sandwich cylinder can significantly affect the global cylinder buckling performance. In the case of the fluted-core sandwich construction, the effective transverse-shear stiffnesses are very different in the directions parallel and perpendicular to the flutes. Parallel to the flutes, the transverse-shear stiffness is primarily a function of the in-plane shear stiffness of the webs and is therefore relatively high in most cases. However, perpendicular to the flutes, the effective transverse-shear stiffness is a function of the bending stiffness of the webs and facesheets, and the rigidity of the web-to-facesheet connection. Thus, the effective transverse-shear stiffness can be relatively low perpendicular to the flutes. Since this perpendicular transverse-shear stiffness is important to characterize, an experimental effort to characterize this property was undertaken. This effort was based on American Society for Testing and Materials (ASTM) C 273, the Standard Test Method for Shear Properties of Sandwich Core Materials.[44] In the C 273 process, a traditional-core material like honeycomb or foam is bonded between relatively rigid steel plates that are attached to hinged grips. As the grips are pulled apart, the core undergoes primarily transverse-shear loading. In fluted-core sandwich composites, the deformation of the facesheets adds to the transverse-shear compliance, so the rigid plates could not be used when trying to determine transverse-shear behavior. Since only curved specimens were available for this study, most of the facesheets were left uncovered and short metal tabs were bonded to the facesheets to introduce the load as shown in Figure 10. These metal plates were custom fabricated to fit an ASTM C 273 hinged fixture. The specimens were 3.0 in. wide and approximately 7 in. long and the hinge pins were 12.53 in. apart. During loading, the deformation was monitored with displacement transducers to measure relative grip position, and with DIC to measure the full-field displacements of the grips, both facesheets, and the edges of the facesheets and webs. Therefore, it was recognized that the specimen design would not directly measure the effective transverse-shear stiffness. However, with this setup a specimen undergoes primarily transverse-shear loading, so the data may be used to verify that FEMs accurately capture the transverse-shear behavior.

The FEM (Figure 11) used the same cross-sectional parameters, geometry, and adjusted material properties as the coupon compression FEM discussed in Section 3.1, given in Table 2, and as more fully described in ref. 39. The FEM had 16,649 shell elements, 8189 nodes, and 47,729 DOF.

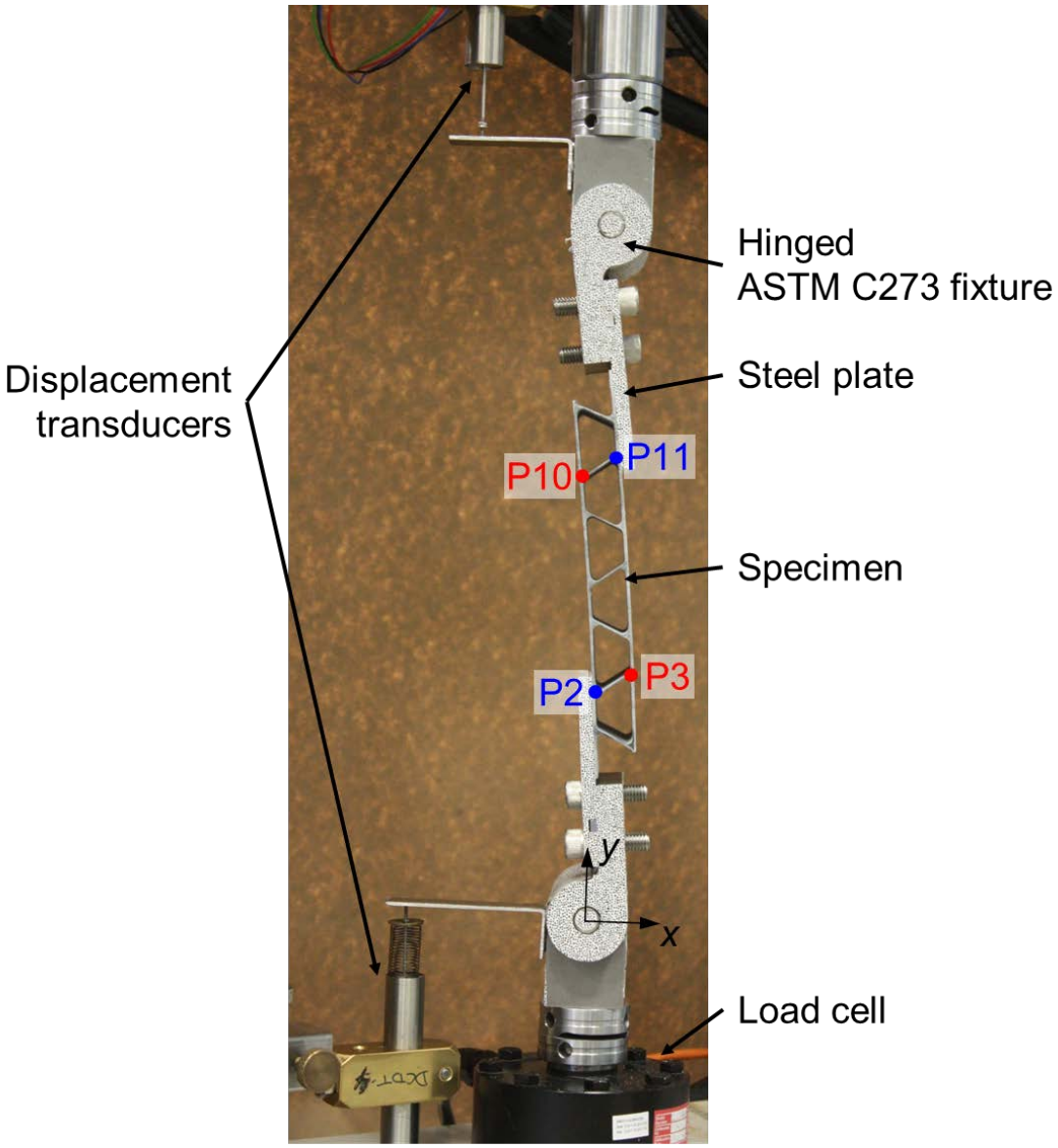


Figure 10. Transverse-shear test setup.

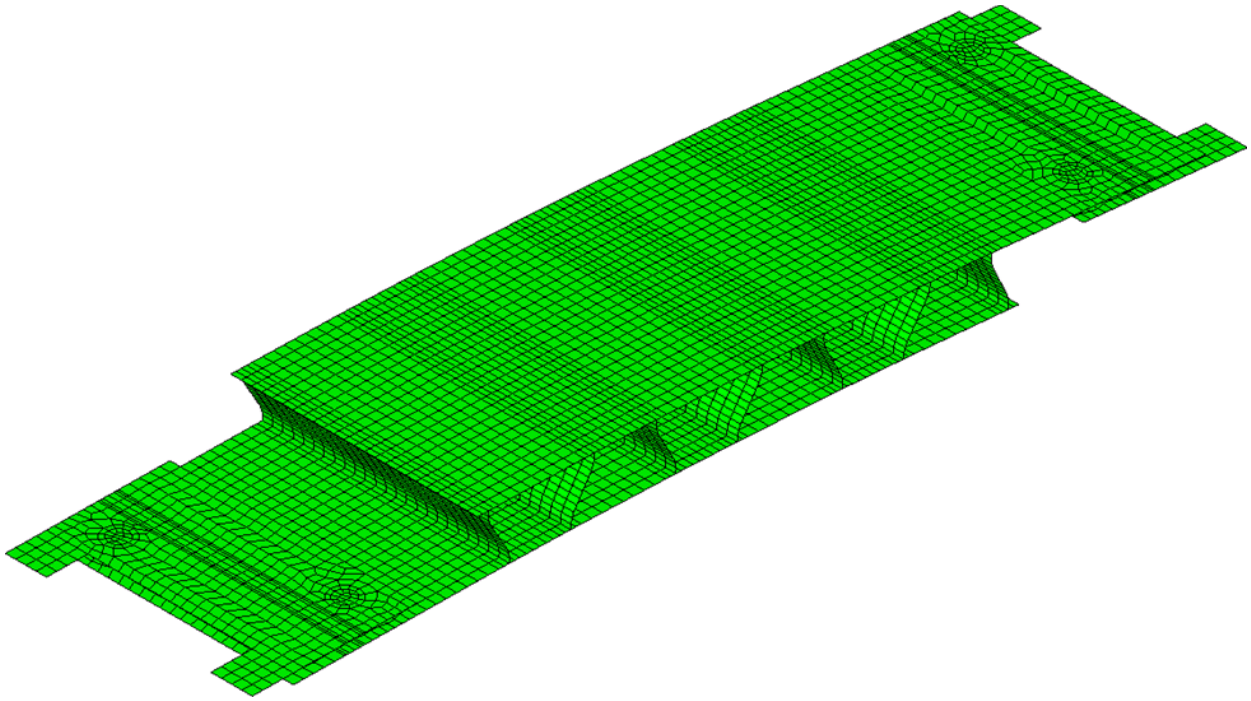


Figure 11. Transverse-shear FEM.

During testing, the bottom fixture with the load cell is held essentially fixed and the load is applied by moving the upper fixture up. The goal with the transverse-shear test was to interrogate the stiffness rather than the strength, so the specimen was loaded to the safe load of 600 lb, then unloaded. When the test was repeated, it was found that there was a hysteretic compliance somewhere in the load train, and the machine and value of the displacement-transducer displacements were not repeatable. Therefore, the specimen was cycled several times in an attempt to reduce this variability. Only the results from the last loading cycle are reported here and the *y*-direction displacements are measured from points directly on the specimen itself. The benefit of measuring the motion points on the specimen itself is that it removes any load-train compliance or slippage that is inevitable with bolted or pinned connections. In this study, the motion of two pairs of noodles was used to characterize the overall specimen stiffness. In particular, the relative *y*-direction (vertical) displacements of the noodles labeled P2 and P11, and P3 and P10 in Figure 10 were used. The relative experimental *y*-displacements measured with DIC for these two pairs (P11 minus P2 and P10 minus P3) are shown in Figure 12 with the P11-P2 displacement shown as the solid blue curve and the P10-P3 displacement shown as the solid red curve. It is seen that the P11-P2 displacement has a positive slope and the P10-P3 displacement has a negative slope. More loading and unloading hysteresis is seen in the experimental P10-P3 displacement than is seen in P11-P2 displacement. The predicted relative displacements are shown as the dashed blue and red curves for the P11-P2 displacement and the P10-P3 displacement, respectively. Though the experimental and predicted displacements were quite similar, based on the displacements at 600 lb, the predicted P11-P2 response was 9% less stiff than the experimental response and the predicted P10-P3 response was 10% more stiff than the experimental response. Because these predictions were similarly softer and stiffer than the test, the average predicted stiffness was well within 1%.

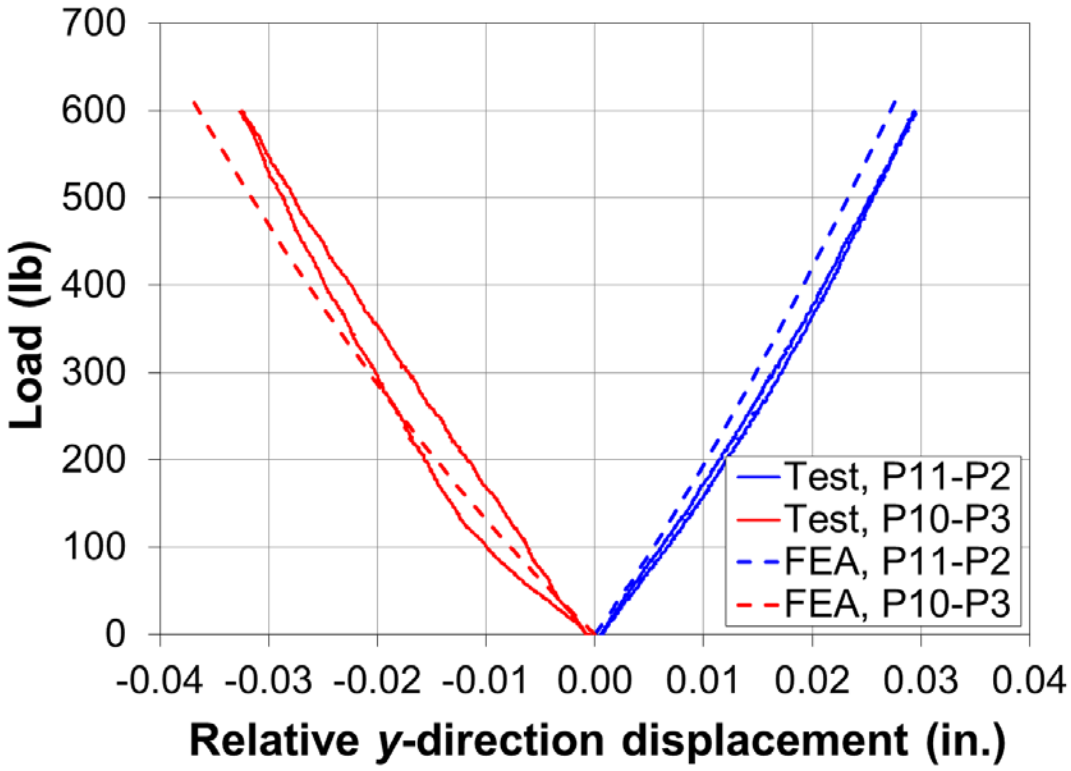
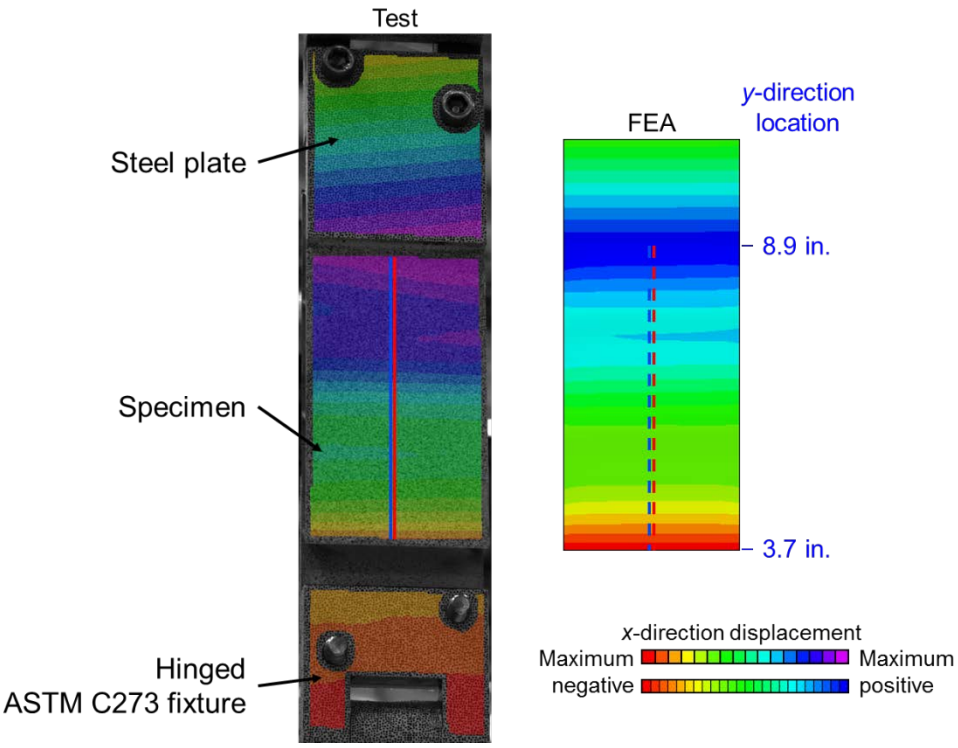
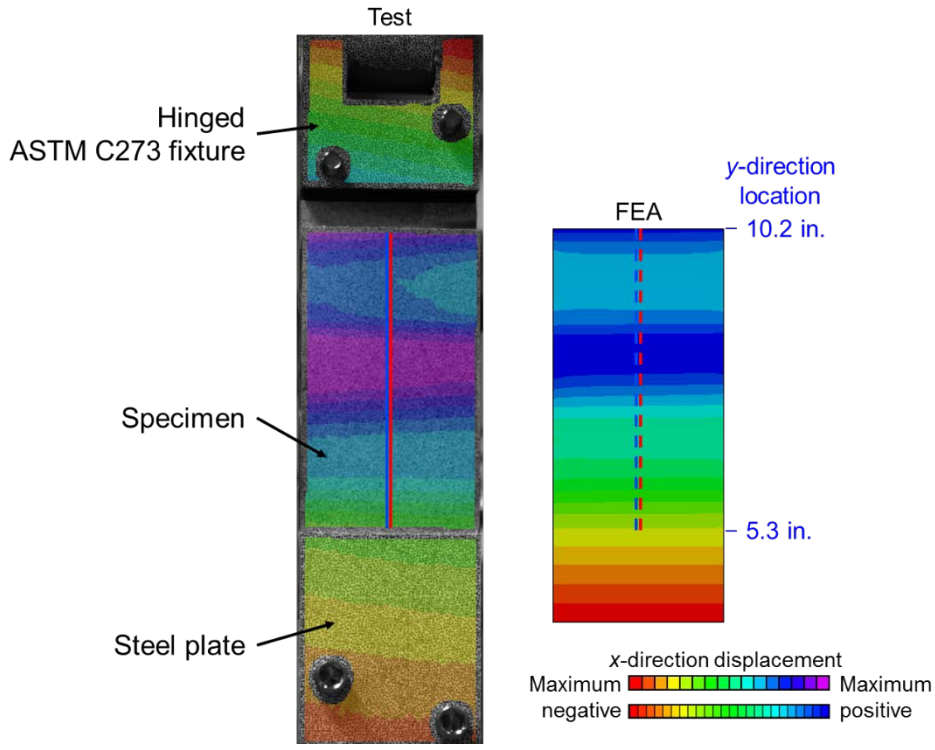



Figure 12. Load versus *y*-direction displacement for the transverse-shear test.

Because much of the effective transverse-shear compliance is due to bending of the facesheets, it is important to also compare measured and predicted *x*-direction displacements to verify that the correct response is being captured in the analysis. The measured and predicted OML and IML *x*-direction (as defined in Figure 10) displacements are shown in a qualitative way by the contour plots in Figure 13 at a load of 600 lb. It is seen that the responses are fairly uniform across the width of the specimen, but it is difficult to compare the displacements even if the values are given in the scales. Instead, the midwidth *x*-direction displacement traces (along the red and blue lines in Figure 13) are shown for two different load levels in Figure 14. In particular, the OML and IML displacements plotted versus the *y*-direction position for loads about 300 lb and 600 lb are shown in Figure 14. To account for rigid-body motion that appeared to occur during test, the *x*-direction displacement for both the OML and IML was shifted by –0.045 in. for the 300-lb load and by –0.052 in. for the 600-lb load. With these shifts in the experimental results, the number, location, and amplitude of the waves in the *x*-direction displacements are very similar between the test and the FEA predictions.

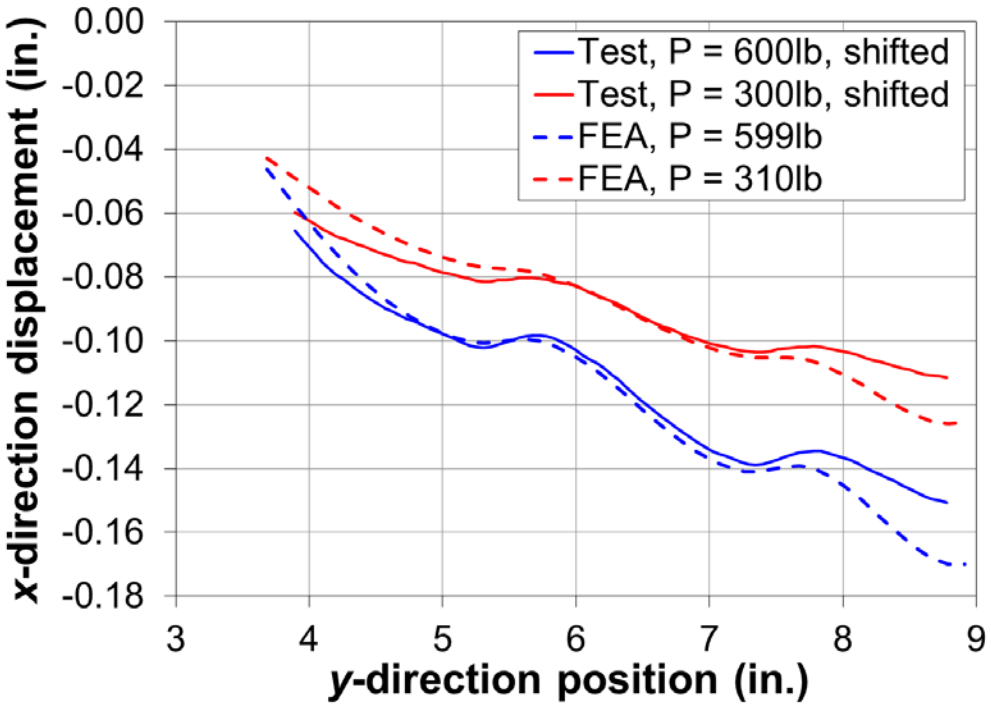



a) OML.

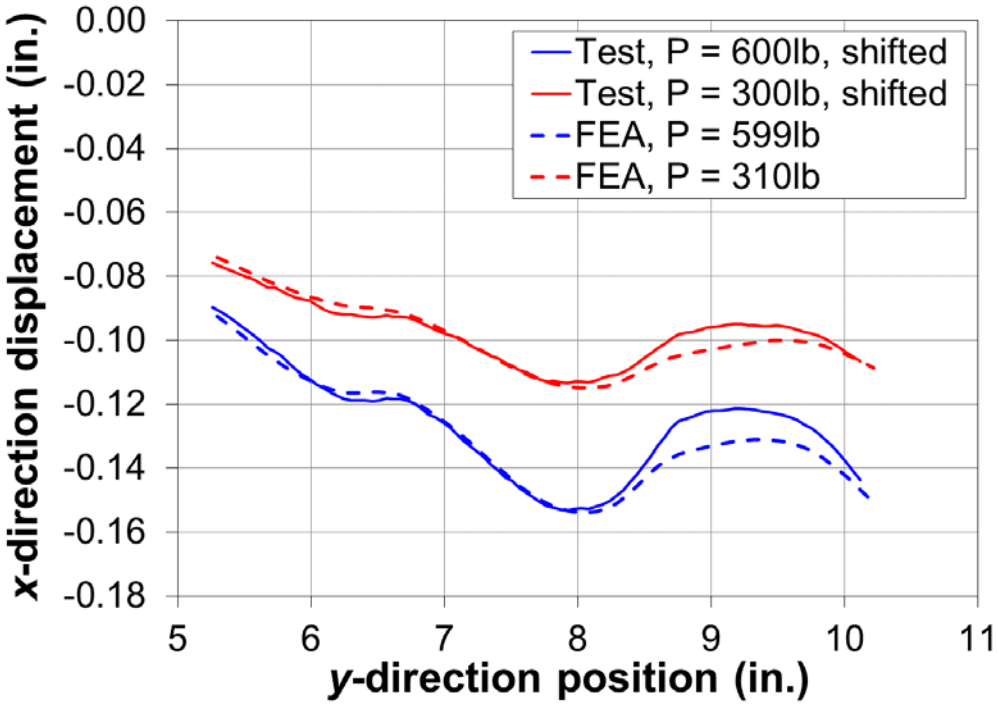



b) IML.

Figure 13. Displacement (*x*-direction) contour plots for the transverse-shear test at the peak for a load of 600 lb.




a) OML.

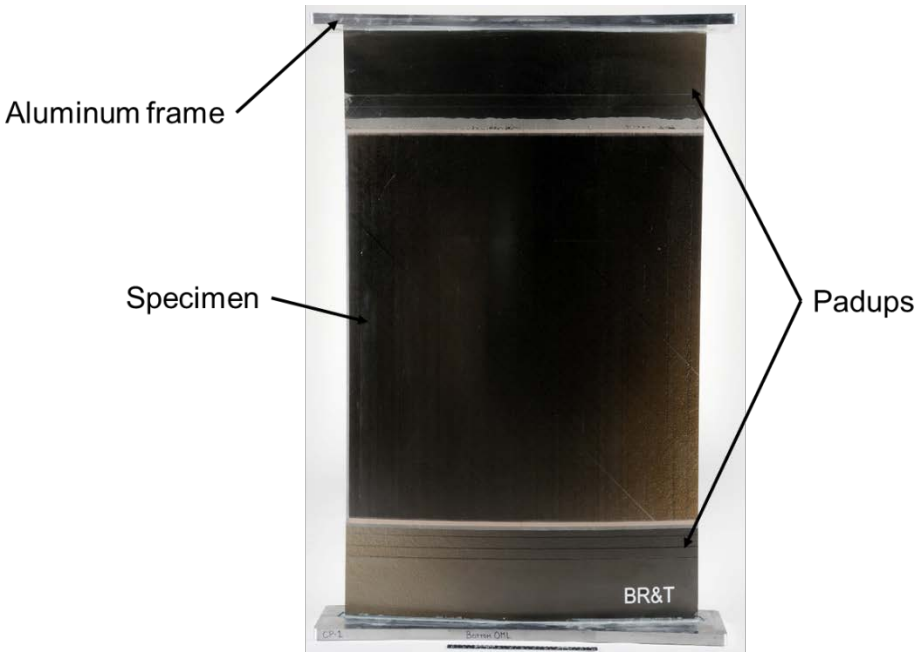



b) IML.

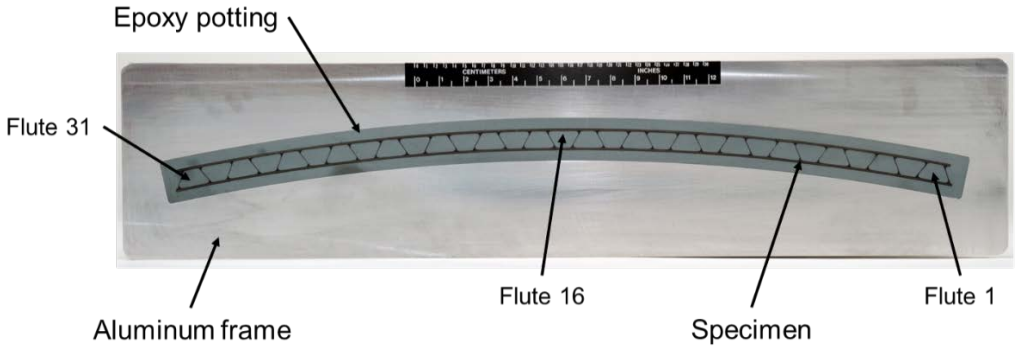
Figure 14. Displacement traces for the transverse-shear test.

### 3.3 Panel Compression Specimens

The final test that was part of this study was an axial compression test of the curved panel, CP-1, shown in Figure 15. This specimen was loaded in displacement control and was designed to buckle out of plane prior to material failure so that the ability of the finite element approach to accurately predict bending behavior could be assessed. The specimen was approximately 54 in. long in the axial direction and about 32 in. wide in the circumferential direction. As shown in Figure 15b, the specimen cross section consisted of 31 flutes. Eight-ply 9.5-in.-long padups were secondarily bonded to the OML and IML at both ends. For the first 6.5 in. near the ends of the panel, the padup had a quasi-isotropic [45/–45/0/90/90/0/–45/45] layup. The outer [90/0] plies were terminated at 6.5 in. from the ends, the remaining [0/90] plies were terminated at 7.5 in., the inner [45/–45] plies were terminated at 8.5 in., and the final [–45/45] plies were terminated at 9.5 in. from the ends. The specimen ends were potted in slotted 8-in.-wide, 36-in.-long, and 1.0-in.-thick aluminum plates with an epoxy grout. Finally, the ends were machined flat.



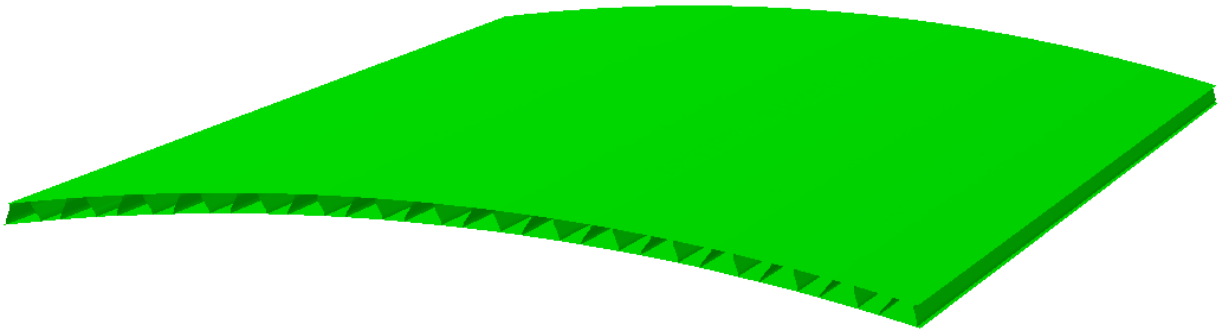

a) OML side view.



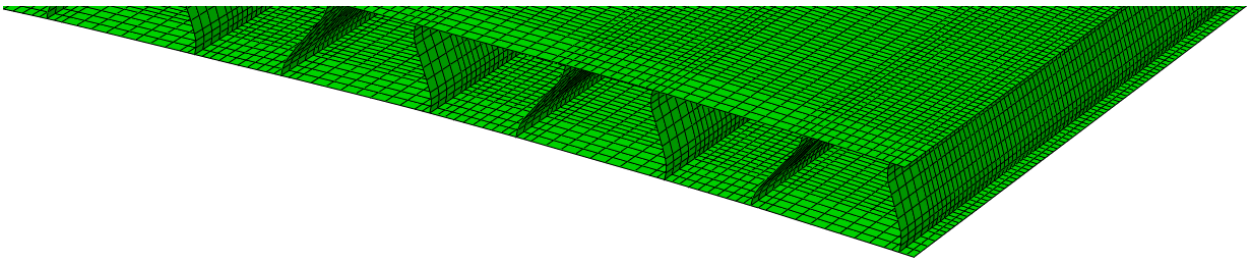

b) Top cross-sectional view.

Figure 15. Panel compression test specimen CP-1.

The panel FEM, shown in Figure 16, used the same cross-sectional parameters and adjusted material properties as the coupon compression FEM given in Table 1 and Table 2. The padups were included in the model by incorporating the additional plies into the existing element properties, so no additional elements or DOF were required. The FEM had 878,618 shell elements, 349,872 nodes, and 2,099,232 DOF.



a) Perspective view of full model (element edges removed).



b) Detail of right-front corner (showing the element edges).

Figure 16. Panel compression FEM.

The load-displacement response of the curved-panel under axial compression is shown in Figure 17. It is seen that the initial response was essentially linear until near the peak load of 121,700 lb where buckling occurs. As the compression displacement was increased, the buckling continued and the load decreased until material failure occurred at a load of 117,000 lb and about 0.16 in. of axial displacement. It is seen that the predicted load-displacement response is very similar to the test. The initial linear stiffnesses matched well and the predicted peak load was 121,400 lb and within 1% of the measured peak load. The largest difference between the test and predicted load-displacement responses appears to be the post-buckled slope. It should be noted that failure was not part of the prediction; in the figure, the analysis response was terminated at an axial displacement similar to that of the experimental failure.

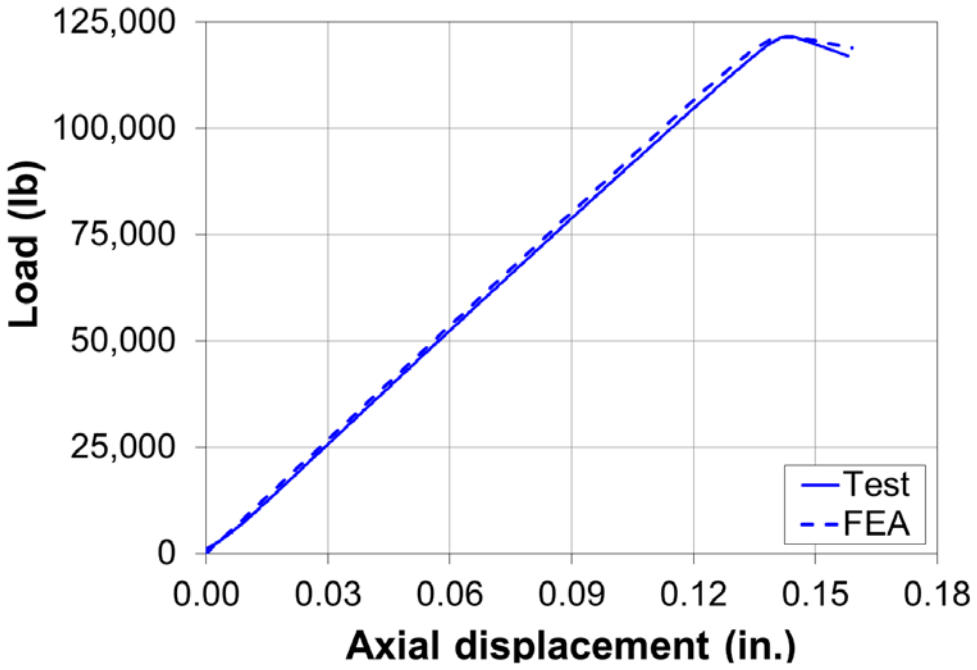
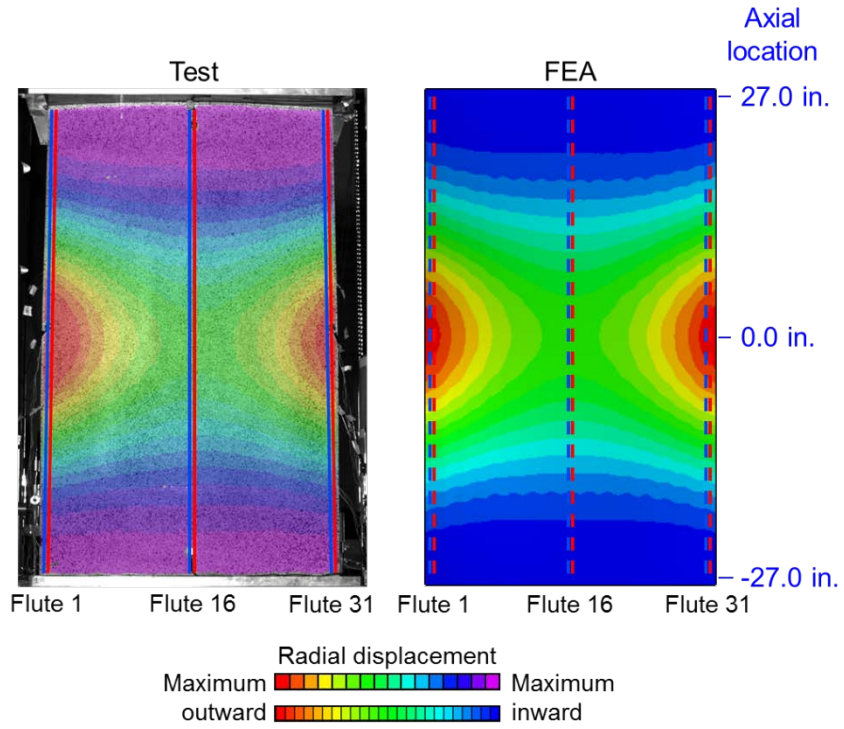
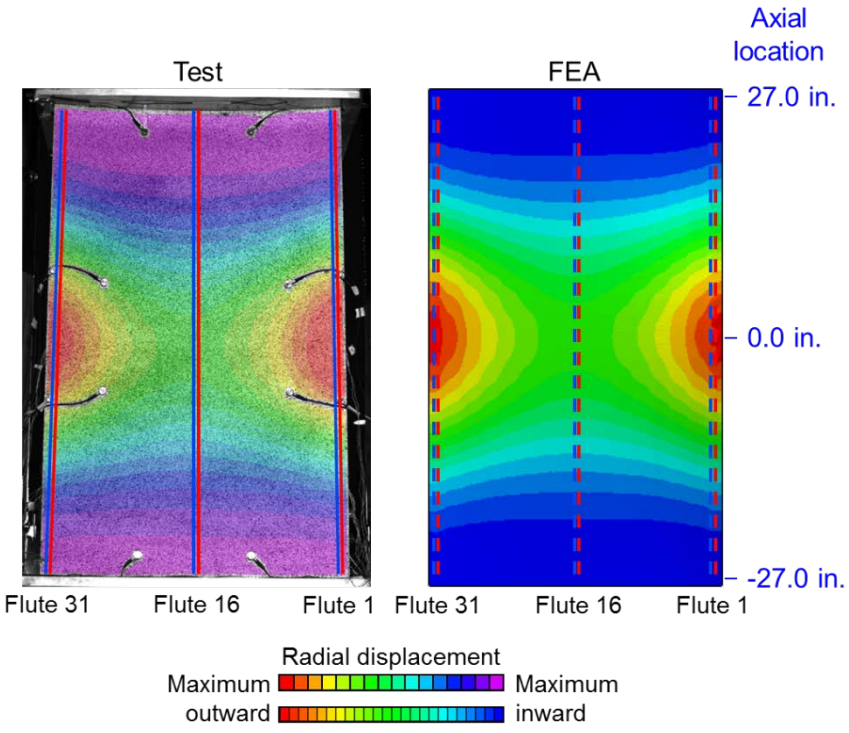



Figure 17. Load versus axial displacement for curved-panel compression specimen CP-1.

To properly validate the finite element approach, it was important to look at the compression response in more detail in addition to the load-displacement curves and peak loads. Therefore, the OML and IML radial-displacement contours near the failure load are shown in Figure 18. The primary radial-displacement response is a global outward deformation of both free edges and the character of this response is very similar between the test and prediction. Also, the qualitative OML and IML responses appear very similar because the panel was designed to undergo global panel buckling. To quantitatively compare the deformations, radial displacement traces along flutes 1, 16, and 31 (Figure 15) are plotted in Figure 19 in blue, red, and green, respectively. (Note that the breaks in the experimental curves are locations where other instrumentation was placed and DIC measurements could not be made.) Considering the test and predictions separately, the maximum flute-16 (midwidth) OML and IML displacements were equal to two significant digits. Specifically, the measured maximum flute-16 IML and OML displacements were 0.47 in.; the predicted maximum flute-16 IML and OML displacements were 0.52 in., which is 11% higher than the test. For the radial displacements in the edge flutes (flutes 1 and 31), the predicted maximum displacements are also greater than the measured displacements. Considering the average of the flute 1 and flute 31 maximum radial displacements, the predicted displacements are 12% greater than the measured on the OML and 14% greater on the IML. Part of the reason that the predicted displacements are consistently higher than the measured displacements may be that the predicted displacements were taken at a load nearly 2000 lb greater than the failure load because that was the solution increment nearest the failure load and the radial displacement in this postbuckled range are highly sensitive to load. Perhaps the most interesting response highlighted by Figure 19 is on the IML in flutes 1 and 31 near the midlength. In this area, it is seen that the displacement traces have a distinct waviness that indicates local face buckling. This local buckling is observed in both the test and the prediction, and the wavelength, amplitudes, and number of half waves are similar in the test and analysis. The fact that this local buckling response on top of the global panel buckling is captured well by the finite element modeling gives confidence that the modeling approach is capable of predicting either global or local responses.

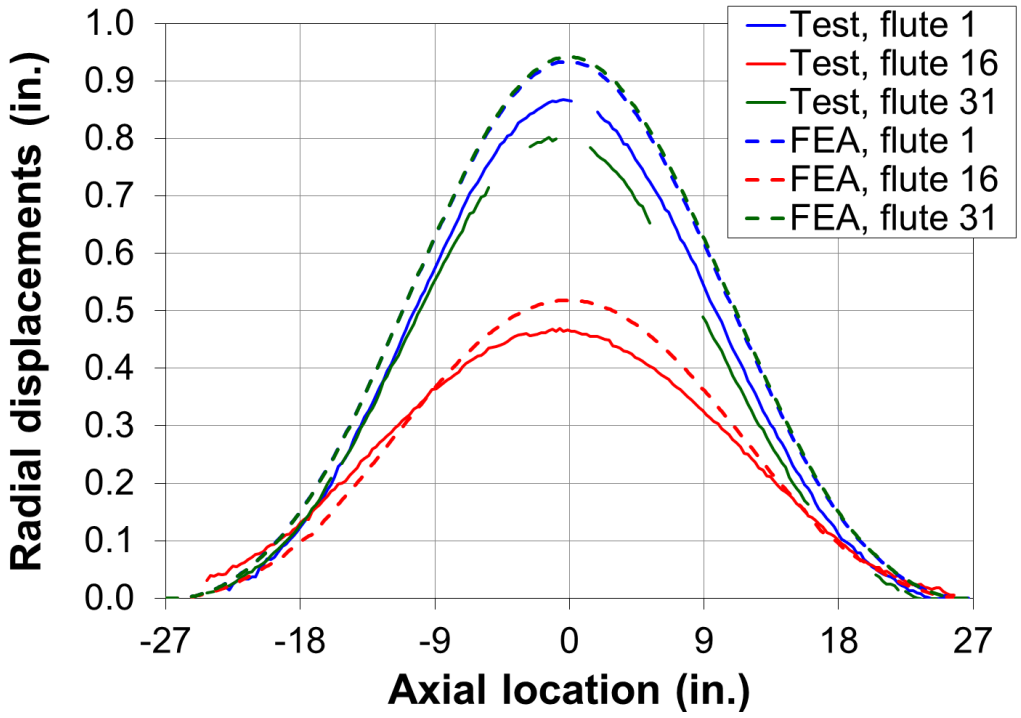



a) OML.

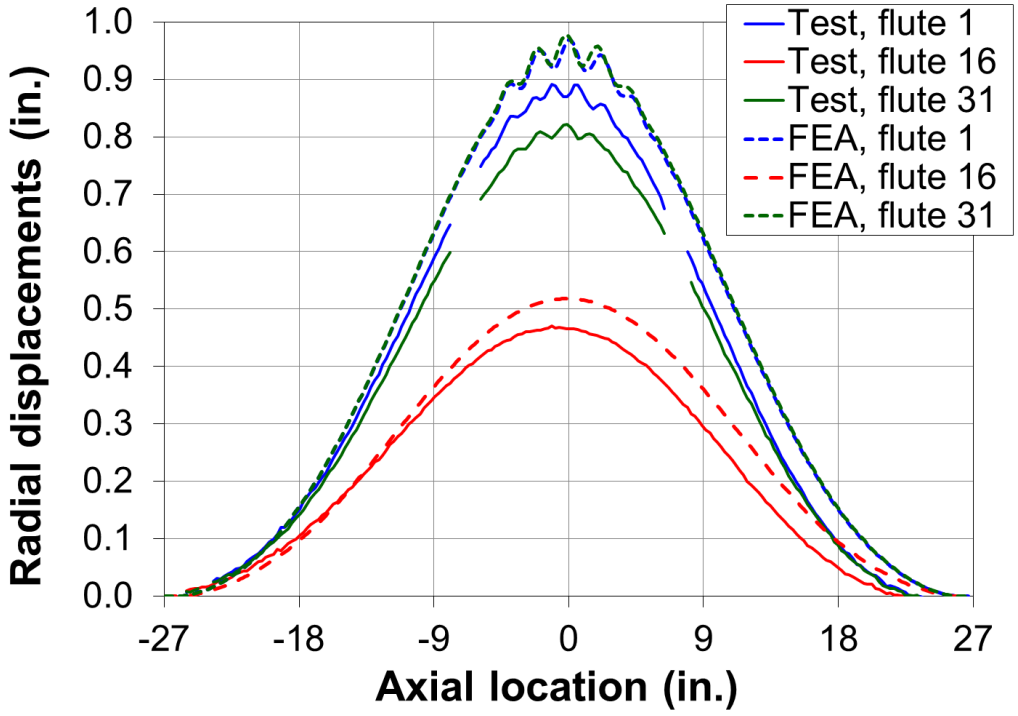



b) IML.

Figure 18. Radial displacement contour plots for the panel compression test at the failure load (117,091 lb for test and 118,938 lb for analysis).




a) OML.




b) IML.

Figure 19. Radial displacement traces for the panel compression test at the failure load (117,091 lb for test and 118,938 lb for analysis).

## 4.0 Concluding Remarks

The use of composite structures for launch vehicle primary structures continues to increase, so it is important to have a good understanding of potential structural responses and to have design and analysis methods capable of capturing these structural responses for any considered structural concept. In this report, a series of structural tests designed specifically to elicit different structural responses—axial compression including local buckling, transverse-shear deformation, and global panel buckling—on fluted-core sandwich composite test articles are detailed and the results are compared with a previously developed FEA approach. After adjusting the material properties used in the analysis to match the stiffness response of the axial compression specimens, the measured and predicted results correlate very well, both in the character of the response and quantitatively. This agreement provides confidence that the developed finite element approach is capable of predicting some of the most important structural responses that this class of fluted-core composite structure are expected to see in launch vehicle applications.

## 5.0 References


1. Caliendo, H.: "Orbital ATK Produces 500th Large Composite Rocket Structure," http://www.compositesworld.com/news/orbital-atk-produces-500th-large-composite-rocket-structure-, Posted on: 4/21/2016.
2. Dawson, D.: "The Emerging Commercial Space Industry," *Composites World*, Volume 2, No. 9, September 2016, pp. 102-111.
3. Dawson, D.: "Size-Unlimited OOA Composite Process Enables Next-Gen Launch System," *Composites World*, Volume 3, No. 1, January 2017, pp. 32-37.
4. Schultz, M. R.; Oremont, L.; Guzman, J. C.; McCarville, D.; Rose, C. A.; and Hilburger, M. W.: "Compression Response of Fluted-Core Composite Panels", *AIAA Journal*, 50(11) (2012) pp. 2546-2557.
5. Shanley, F. R.: "Cardboard-Box Wing Structures," *Journal of Aeronautical Sciences*, Volume 14, Number 12, December 1947, pp. 713-715.
6. Lampert, S. and Younger, D. G.: *Multi-Wall Structures for Space Vehicles*, Wright Air Development Division, WADD Technical Report 60-503, May 1960.
7. Libove, C. and Hubka, R. E.: *Elastic Constants for Corrugated-Core Sandwich Plates*, NACA TN 2289, February 1951.
8. Seide, P.: *The Stability Under Longitudinal Compression of Flat Symmetric Corrugated-Core Sandwich Plates with Simply Supported Loaded Edges and Simply Supported or Clamped Unloaded Edges*, NACA TN 2679, April 1952.
9. Younger, D. G. and Lampert, S.: *An Experimental Study on Multi-Wall Structures for Space Vehicles*, Wright Air Development Division, WADD Technical Report 60-800, March 1961.
10. Petersen, J. P. and Anderson, J. K.: *Test of a Truss-core Sandwich Cylinder Loaded to Failure in Bending*, NASA TN D-3157, December 1965.
11. Anderson, M. S.: *Local Instability of the Elements of a Truss-Core Sandwich Plate*, NASA TR R-30, 1959.

12. Fung, T. C.; Tan, K. H.; and Lok, T. S.: "Shear Stiffness DQy for C-Core Sandwich Panels," *Journal of Structural Engineering*, Vol. 122, No. 8, August, 1996, pp. 958-966.

13. Fung, T. C; and Tan, K. H.: "Shear Stiffness for Z-Core Sandwich Panels," *Journal of Structural Engineering*, Vol. 124, No. 7, July, 1998, pp. 809-816.

14. Lok, T. S.; Cheng, Q.; and Heng, L.: "Equivalent Stiffness Parameters of Truss-Core Sandwich Panel," *Proceedings of the Ninth International Offshore and Polar Engineering Conference*, Brest, France, May 30 – June 4, 1999, pp. 292-298.

15. Lok, T. S. and Cheng, Q.: "Elastic Stiffness Properties and Behavior of Truss-Core Sandwich Panel," *Journal of Structural Engineering*, Vol. 126, No. 5, May, 2000, pp. 552-559.

16. Romanoff, J.; Remes, H.; Socha, G.; Jutila, M.; and Varsta, P.: "The Stiffness of Laser Stake Welded T-Joints in Web-Core Sandwich Structures," *Thin-Walled Structures*, Vol. 45, 2007, pp. 453-462.

17. Romanoff, J. and Varsta, P.: "Bending Response of Web-Core Sandwich Plates," *Composite Structures*, Vol. 81, 2007, pp. 292-302.

18. Jegley, D. C.: *A Study of the Structural Efficiency of Fluted Core Graphite-Epoxy Panels*, NASA/TM–1990-101681, January 1990.

19. Collier, C. S.: "Stiffness, Thermal Expansion, and Thermal Bending Formulation of Stiffened, Fiber-Reinforced Composite Panels," *Proceedings of the 34th AIAA/ASME/ASCE/AHS/ASC Structures, Structural Dynamics, and Materials Conference*, AIAA paper no. AIAA-93-1569, La Jolla, CA, April 1993.

20. Collier, C. S.: "Thermoelastic Formulation of Stiffened, Unsymmetric Composite Panels for Finite Element Analysis of High Speed Aircraft," *Proceedings of the 35th AIAA/ASME/ASCE/AHS/ASC Structures, Structural Dynamics, and Materials Conference*, AIAA paper no. AIAA-94-1579, Hilton Head, SC, April 1994.

21. Martinez, O.; Bapanapalli, S.; Sankar, B.; Hafka, R.; and Blosser, M.: "Micromechanical Analysis of Composite Truss-Core Sandwich Panels for Integral Thermal Protection Systems," *Proceedings of the 47th AIAA/ASME/ASCE/AHS/ASC Structures, Structural Dynamics, and Materials Conference*, AIAA paper no. AIAA 2006-1876, Newport, RI, May 2006.

22. Martinez, O. A.; Sankar, B. V.; Hafka, R. T.; Bapanapalli, S. K.; and Blosser, M. L.: "Micromechanical Analysis of Composite Corrugated-Core Sandwich Panels for Integral Thermal Protection Systems," *AIAA Journal*, Vol. 45, No. 9, September 2007.

23. Sharma, A.; Sankar, B. V.; and Haftka, R. T.: "Homogenization of Plates with Microstructure and Application to Corrugated Core Sandwich Panels," *Proceedings of the 51st AIAA/ASME/ASCE/AHS/ASC Structures, Structural Dynamics, and Materials Conference*, AIAA paper no. AIAA 2010-2706, Orlando, FL, April 2010.

24. Kothari, A. P.; Livingston, J. W.; Tarpley, C.; Raghavan, V.; Bowcutt, K. G.; and Smith, T. R.: "A Reusable, Rocket and Airbreathing Combined Cycle Hypersonic Vehicle Design for Access-to-Space," *Proceedings for the AIAA Space 2010 Conference & Exposition*, AIAA paper no. AIAA 2010-8905, Anaheim, CA, August-September 2010.

25. Boorle, R. K. and Mallick, P. K.: "Global Bending Response of Composite Sandwich Plates with Corrugated Core. Part I: Effect of Geometric Parameters," *Composite Structures,* Vol. 141, 2016, pp. 375-388.

26. Boorle, R. K. and Mallick, P .K.: "Global Bending Response of Composite Sandwich Plates with Corrugated Core. Part II: Effect of Laminate Construction," *Composite Structures,* Vol. 141, 2016, pp. 389-402.

27. Dayyani, I.; Shaw, A. D.; Saavedra Flores, E. I.; and Friswell, M. I.: "The Mechanics of Composite Corrugated Structures: A Review with Applications in Morphing Aircraft," *Composite Structures,* Vol. 133, 2015, pp. 358-380.

28. Zangani, D.; Robinson, M.; and Gibson, A. G.: "Evaluation of Stiffness Terms for Z-Cored Sandwich Panels," *Applied Composite Materials,* Vol. 14, No. 3, May 2007, pp. 159-175.

29. Benarcyck, B. A.; Arnold, S. M.; and Hopkins, D. A.: "Design of Fiber Reinforced Foam Sandwich Panels for Large Ares V Structural Applications," *Proceedings of the 51st AIAA/ASME/ASCE/AHS/ASC Structures, Structural Dynamics, and Materials Conference*, AIAA paper no. AIAA 2010-2781, Orlando, FL, April 2010.

30. Tumino, D.; Ingrassia, T.; Nigrelli, V.; Pitarresi, G.; and Urso Miano, V.: "Mechanical Behavior of a Sandwich with Corrugated GRP Core: Numerical Modeling and Experimental Validation," *Frattura ed Integrità Strutturale,* Vol. 30, 2014, pp. 317-326.

31. McCarville, D.; Guzman, J. C.; Sweetin, J.; Jackson, J.; Pelham, L.; Steensland, J.; Soden, M.; and Peterson, C.: "Manufacturing Overview of a 2.4 Meter (7.9 Foot) Composite Cryotank," *SAMPE Journal*, Volume 49, No. 5, September/October 2013, pp. 7-13.

32. McCarville, D.: "Fabrication of Large Scale Fluted Core Co-Bonded Composite Structure," *National Space and Missile Materials Symposium*, Huntsville, AL, June 2014.

33. Tidwell, R. S.; McCarville, D. A.; Birkland, J. O.; and Guzman, J. C.: "Fluted Core Skirt Development for the Composite Cryotank Technology Development Program," *SAMPE Conference Proceedings*, Seattle, WA, June 2-5, 2014

34. Sleight, D. W.; Rosario, S.; Johnson, T. F.; and Shular, D. A.: Composite Cryotank Technology Demonstration 5.5-Meter Diameter Pre-Test Analysis and Test Readiness, NASA/TM–2016-219325, July 2016.

35. Hilburger M. W.: "Developing the Next Generation Shell Buckling Design Factors and Technologies," *Proceedings of the 53rd AIAA/ASME/ASCE/AHS/ASC Structures, Structural Dynamics, and Materials Conference*, AIAA paper no. AIAA 2012-1686, Honolulu, HI, April 2012.

36. Stein, M.; and Mayers, J.: *Compressive Buckling of Simply Supported Curved Plates and Cylinders of Sandwich Construction*, NACA TN 2601, 1952.

37. Lovejoy, A. E.; and Schultz, M. R.: "Evaluation of Analysis Techniques for Fluted-Core Sandwich Cylinders," *Proceedings of the 53rd AIAA/ASME/ASCE/AHS/ASC Structures, Structural Dynamics & Materials Conference*, AIAA paper no. 2012-1868, Honolulu, HI, April 2012.

38. Oremont, L. and Schultz, M. R.: "An Efficient Analysis Methodology for Fluted-Core Composite Structures," *Proceedings of the 53rd AIAA/ASME/ASCE/AHS/ASC Structures,*

*Structural Dynamics & Materials Conference*, AIAA paper no. 2012-1867, Honolulu, HI, April 2012.

39. Oremont, L.; and Schultz, M. R., Guzman, J. C., McCarville, D., and Hilburger, M. W.: *Modeling and Analysis of Fluted-Core Composite Structures for Aerospace Applications*, NASA/TM-20210000641, January 2021.
40. Schultz, M. R.; Rose, C. A.; Guzman, J. C.; McCarville, D.; and Hilburger, M. W.: "An Experimental Study of the Compression Response of Fluted-Core Composite Panels with Joints," *Composites Part B: Engineering*, Vol. 61, May 2014.
41. Sutton, M. A.; Orteu, J.-J.; and Schreier, H. W.: *Image Correlation for Shape, Motion and Deformation Measurements: Basic Concepts, Theory and Applications*, Springer, New York, 2009.
42. Patran® 2014, Software Package, MSC Software Corporation, Santa Ana, CA, 2014.
43. Abaqus/Standard, Software Package, Ver. 6.13-3, Dassault Systèmes, Waltham, MA, 2013.
44. Anonymous, ASTM Standard C 273/C 273M-07a, *Standard Test Method for Shear Properties of Sandwich Core Materials*, ASTM International, West Conshohocken, PA, 2007.

# REPORT DOCUMENTATION PAGE

*Form Approved*
*OMB No. 0704-0188*

The public reporting burden for this collection of information is estimated to average 1 hour per response, including the time for reviewing instructions, searching existing data sources, gathering and maintaining the data needed, and completing and reviewing the collection of information. Send comments regarding this burden estimate or any other aspect of this collection of information, including suggestions for reducing the burden, to Department of Defense, Washington Headquarters Services, Directorate for Information Operations and Reports (0704-0188), 1215 Jefferson Davis Highway, Suite 1204, Arlington, VA 22202-4302. Respondents should be aware that notwithstanding any other provision of law, no person shall be subject to any penalty for failing to comply with a collection of information if it does not display a currently valid OMB control number.
**PLEASE DO NOT RETURN YOUR FORM TO THE ABOVE ADDRESS.**

| 1. REPORT DATE *(DD-MM-YYYY)* | 2. REPORT TYPE | 3. DATES COVERED *(From - To)* |
|---|---|---|
| 01/01/2021 | TECHNICAL MEMORANDUM | February 2013 - March 2017 |

**4. TITLE AND SUBTITLE**
Experimental and Analytical Characterization of Fluted-Core Sandwich Composite Structures

**5a. CONTRACT NUMBER**

**5b. GRANT NUMBER**

**5c. PROGRAM ELEMENT NUMBER**

**6. AUTHOR(S)**
Schultz, Marc R.; Oremont, Leonard; Gardner, Nathaniel W.; Guzman, J. Carlos; McCarville, Douglas; Hilburger, Mark W.

**5d. PROJECT NUMBER**

**5e. TASK NUMBER**

**5f. WORK UNIT NUMBER**
869021.04.23.01.13

**7. PERFORMING ORGANIZATION NAME(S) AND ADDRESS(ES)**
NASA Langley Research Center
Hampton, VA 23681-2199

**8. PERFORMING ORGANIZATION REPORT NUMBER**

**9. SPONSORING/MONITORING AGENCY NAME(S) AND ADDRESS(ES)**
National Aeronautics and Space Administration
Washington, DC 20546-001

**10. SPONSOR/MONITOR'S ACRONYM(S)**
NASA

**11. SPONSOR/MONITOR'S REPORT NUMBER(S)**
NASA/TM-20210000643

**12. DISTRIBUTION/AVAILABILITY STATEMENT**
Unclassified - Unlimited
Subject Category
Availability: NASA STI Program (757) 864-9658

**13. SUPPLEMENTARY NOTES**
The work described was part of the NASA Engineering and Safety Center (NESC) Shell Buckling Knockdown Factor Project, NESC assessment number 07-010-E. The considered test articles were fabricated by The Boeing Company.

**14. ABSTRACT**

Fluted-core sandwich composite structures, which consist of facesheets separated by angled web members, are potentially advantageous for aerospace structures. However, they can exhibit local buckling and transverse-shear behaviors that can have a large influence on material failure and global buckling, respectively. In this report, a series of experiments designed to elicit some of these fluted-core sandwich composite structural responses is discussed and the results are compared with results from a previously developed finite element analysis approach; qualitative and quantitative agreement between the experiment and analysis is shown.

**15. SUBJECT TERMS**
Fluted-core sandwich composite structures, finite element analysis, structural modeling

| 16. SECURITY CLASSIFICATION OF: | | | 17. LIMITATION OF ABSTRACT | 18. NUMBER OF PAGES | 19a. NAME OF RESPONSIBLE PERSON |
|---|---|---|---|---|---|
| a. REPORT | b. ABSTRACT | c. THIS PAGE | | | HQ - STI-infodesk@mail.nasa.gov |
| U | U | U | UU | 36 | 19b. TELEPHONE NUMBER *(Include area code)* 757-864-9658 |